

Selection of Source Images Heavily Influences the Effectiveness of Adversarial Attacks

Utku Ozbulak Esla Timothy Anzaku Wesley De Neve
Ghent University, Belgium

{utku.ozbulak, eslatimothy.anzaku, wesley.deneve,}@ugent.be

Arnout Van Messem
University of Liège, Belgium

arnout.vanmessem@uliege.be

Abstract

Although the adoption rate of deep neural networks (DNNs) has tremendously increased in recent years, a solution for their vulnerability against adversarial examples has not yet been found. As a result, substantial research efforts are dedicated to fix this weakness, with many studies typically using a subset of source images to generate adversarial examples, treating every image in this subset as equal. We demonstrate that, in fact, not every source image is equally suited for this kind of assessment. To do so, we devise a large-scale model-to-model transferability scenario for which we meticulously analyze the properties of adversarial examples, generated from every suitable source image in ImageNet by making use of two of the most frequently deployed attacks. In this transferability scenario, which involves seven distinct DNN models, including the recently proposed vision transformers, we reveal that it is possible to have a difference of up to 12.5% in model-to-model transferability success, 1.01 in average L_2 perturbation, and 0.03 (8/225) in average L_∞ perturbation when 1,000 source images are sampled randomly among all suitable candidates. We then take one of the first steps in evaluating the robustness of images used to create adversarial examples, proposing a number of simple but effective methods to identify unsuitable source images, thus making it possible to mitigate extreme cases in experimentation and support high-quality benchmarking.

1. Introduction

Thanks to recent advances in the field of deep neural networks, a wide range of problems that were once thought to be hard challenges found easy-to-adopt solutions [33, 56]. Indeed, many deep learning libraries now come with built-in solutions and pre-trained models, further increasing the adoption rate of such networks in the area of computer vision [1, 28, 45]. In spite of receiving a large amount of research attention, a number of fundamental flaws of DNNs still remain unsolved. One of those flaws is their vulnera-

bility to adversarial attacks, where small changes in inputs may lead to large changes in predictions [53].

Although adversarial attacks have been recognized to be a threat for all domains that make use of DNNs, the domain of vision in particular is said to be the one that suffers from adversarial attacks the most, since the perturbation is often invisible to the bare eye. Moreover, continuous deployment of DNNs for mission-critical tasks such as self-driving cars and medical diagnosis tools further amplify this threat since the adversarial examples are not easily detectable [10, 17, 40, 57]. In order to find solutions for this weakness, many studies investigate the adversarial threat from two angles: adversarial attacks and adversarial defenses [5, 52, 63]. In this framework, novel adversarial attacks aim at finding more efficient perturbation generation methods whereas defenses try to prevent or detect as many adversarial examples as possible.

In recent years, numerous adversarial defenses were proposed in order to prevent or detect adversarial examples [20, 31, 37, 46]. Proposed defenses often claim a certain level of robustness against adversarial examples that have an amount of perturbation less than a selected norm [12]. Since the topic of adversariality is closely linked with security, reproducibility of newly proposed techniques is of utmost importance. As a result, there have been a number of impactful studies that analyze the correctness and reliability of newly proposed adversarial defenses [2, 3, 7, 54]. In this context, Carlini and Wagner [7], for instance, demonstrated that most of the defenses proposed for MNIST [35] do not even generalize to CIFAR [32]. This observation prompted research on the suitability of datasets for adversarial research [36], with Carlini and Wagner further suggesting that the usage of larger datasets such as ImageNet [48] may be necessary given the lack of generalization of defenses proposed for smaller datasets [7].

Even though the results obtained with ImageNet are more convincing, working with ImageNet is much more challenging than, for example, working with MNIST or CIFAR. Indeed, not only does ImageNet contain more images than the other two, the images themselves are also larger.

In addition, DNNs that achieve state-of-the-art results for ImageNet are also much bigger than their counterparts that achieve state-of-the-art results for MNIST or CIFAR, thus posing a challenge in terms of computational power needed. As a result, most of the studies that work with ImageNet only use a subset of images in order to create adversarial examples, unless that research is performed by a large industry lab that can afford the computational power (see Figure 1).

Although the studies of [51, 54] hinted that not all source images may be equally suitable for adversarial example creation, most of the studies that work with adversarial examples often randomly sample source images among the ones that are correctly classified. As such, any image that is correctly classified by the models of interest is thought to be suitable and equal in terms of model-to-model transferability, as well as required perturbation to achieve adversariality. To the best of our knowledge, an in-depth analysis on source image suitability of adversarial examples in large-scale model-to-model scenarios has not been conducted yet. Hence, approaching the problem of adversarial examples from a different angle and following the directions of [18, 51, 54], instead of analyzing the effectiveness of attacks, the durability of defenses, or the robustness of models, our study focuses on the source images used to create adversarial examples, hereby investigating the impact of image selection on (1) the success of model-to-model adversarial transferability and (2) the required perturbation to achieve this transferability.

With the help of large-scale experiments, using two of the most prominent attacks in the field as well as 7 different DNNs, including the recently proposed vision transformers, we make the following contributions:

- We reveal that even when the most-studied adversarial attacks for benchmarking are used, model-to-model transferability successes of adversarial examples, as well as the amount of required perturbation to achieve this transferability, heavily depend on the source images used to create those adversarial examples.
- In light of the experiments on model-to-model transferability, we expose the fragility of a subset of images that achieve unnaturally high model-to-model adversarial transferability with comparably low perturbation budgets. Moreover, we show that these fragile images also become “adversarial examples” when making use of non-adversarial noise.
- We present a case study, hereby showing how the experimental results obtained may lead to misleading conclusions when making use of certain subsets of source images.
- We take one of the first steps to identify the aforementioned fragile source images, proposing a set of

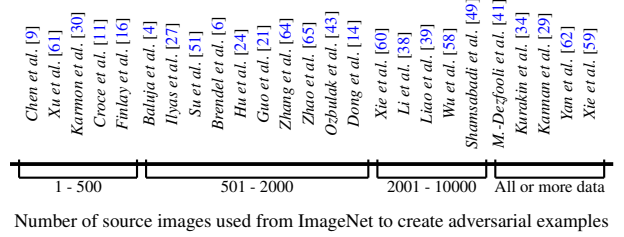


Figure 1: A number of studies that work with images taken from the ImageNet validation set, grouped based on the number of source images used for creating adversarial examples.

suggestions for conducting high-quality experiments in this area and discussing a number of additional findings that can serve as inspiration for future research directions.

2. Adversarial attacks

Assuming an M -class setting in which a data point and its categorical association are defined as $\mathbf{x} \in \mathbb{R}^k$ and $\mathbf{y} \in \mathbb{R}^M$, respectively, with $y_c = 1$ and $y_m = 0, \forall m \in \{0, \dots, M\} \setminus \{c\}$, let g be a classification function that maps inputs onto categorical predictions. In this setting, we define the output $g(\theta, \mathbf{x}) \in \mathbb{R}^M$ as the logits obtained by a prediction model/classifier using the parameters θ . The given data point is then classified into the category with the largest logit value: $G(\theta, \mathbf{x}) = \arg \max_t (g(\theta, \mathbf{x})_t)$. If $G(\theta, \mathbf{x}) = \arg \max_t (y_t)$, then this classification is correct.

For the given setting, a perturbation $\Delta_{\mathbf{x}}$ bounded by the L_p ball centered at \mathbf{x} with a radius ϵ ,

$$\mathcal{B}(\mathbf{x})_{\epsilon}^p := \{\hat{\mathbf{x}} : \|\Delta_{\mathbf{x}}\|_p := \|\mathbf{x} - \hat{\mathbf{x}}\|_p \leq \epsilon\}, \quad (1)$$

is said to be an *adversarial perturbation* if $G(\theta, \mathbf{x}) \neq G(\theta, \hat{\mathbf{x}})$. In this case, $\hat{\mathbf{x}}$ is said to be an adversarial example.

Since the discovery of adversarial examples, a plethora of attacks using a wide range of perturbation generation methods has been proposed [47, 42, 61]. Early research efforts made use of three different attacks for defense evaluation purposes: L-BFGS optimization [53], Fast Gradient Sign (FGS) [19], and Iterative Fast Gradient Sign (IFGS) [34]. The authors of [8] showed that the three aforementioned attacks create adversarial examples that are trivial to detect or defend against and proposed the usage of Carlini & Wagner’s Attack (CW) for the evaluation of defenses. Although in their subsequent research efforts, the authors of [8] preferred the use of a variety of different attacks, they often start analyzing the robustness of defences with two attacks: the Projected Gradient Descent attack (PGD) [54] and CW. In recent years, these two attacks have

become standard approaches for evaluating adversarial robustness in many studies. Following these findings, the study presented in this paper also uses these two attacks for examining the fragility of source images.

PGD can be seen as a generalization of FGS and IFGS. In particular, this attack aims at finding an adversarial example \hat{x} that satisfies $\|\hat{x} - x\|_\infty < \epsilon$, where the perturbation is defined within an L_∞ ball centered at x with a radius ϵ . The adversarial example is iteratively generated as:

$$[\hat{x}]_{n+1} = \Pi_\epsilon([\hat{x}]_n - \alpha \text{sign}(\nabla_x J(g(\theta, [\hat{x}]_n)_c))), \quad (2)$$

with $[\hat{x}]_1 = x$, where the perturbation is calculated using the signature of the gradient of the cross-entropy loss, $\text{sign}(\nabla_x J(g(\theta, [\hat{x}])_c))$, originating from the target class c . In this setting, α controls the exercised perturbation at each iteration and Π_ϵ is a function that controls the L_∞ limit imposed on the perturbation.

CW, on the other hand, is a complex attack that uses L_2 as follows:

$$\min_{\hat{x}} f(\hat{x}, c) + \|\hat{x} - x\|_2, \quad (3)$$

where f is a preferred loss function. We follow [8, 51] and use the following loss:

$$f(\hat{x}, c) = \max_k \{ \max_{c \neq k} \{ g(\theta, \hat{x})_c - g(\theta, \hat{x})_k \} - \kappa \}, \quad (4)$$

where the target class is selected with c and the confidence of the attack is adjusted with κ .

Given that adversarial examples are trivial to generate in white-box cases [2, 7], and given the recent focus on the importance of adversarial evaluation in black-box scenarios [27, 55], our study mainly focuses on analyzing the properties of adversarial examples that achieve model-to-model transferability. In this context, an adversarial example created by a model is said to achieve model-to-model adversarial transferability if it is also incorrectly classified by another model, provided that the source image used to create the adversarial example is initially correctly classified by both models.

3. Experimental setup

Models—In this study, we use five different deep learning architectures that see frequent use in the literature. The considered models are: AlexNet [33], SqueezeNet [26], VGG-16 [50], ResNet-50 [23], and DenseNet-121 [25]. In addition to these models, we also include two recently proposed vision transformer models, Vision Transformer Base/16–224 (ViT-B) and Vision Transformer Large/16–224 (ViT-L), which achieve state-of-the-art results on ImageNet [15]. From here on, each model will be denoted by its set of parameters $\theta_i, i \in \{1, \dots, 7\}$, and multiple models will be denoted by $\Theta = \{\theta_1, \dots, \theta_7\}$.

Data—We follow the approach used by previous studies on adversariality, leveraging the images in the ImageNet validation set for generating adversarial examples. In this paper, these unperturbed images are referred to as *source images*. Further adopting previously used methods, we only rely on images that are correctly classified by all selected models in order to conduct trustworthy experiments on adversarial transferability, thus ensuring $G(\theta_i, x) = \arg \max_t (y_t), \forall i \in \{1, \dots, 7\}$. By doing so, we filter out images that are hard to correctly classify for at least one of our models, thus limiting the hypothesis space and allowing us to perform a best-case analysis. After this filtering operation, we are left with a set of 19,025 source images, which approximately corresponds to 38% of the ImageNet validation set. We will refer to this set of 19,025 source images as:

$$\mathbb{S} = \{x \mid G(\theta_i, x) = \arg \max_t (y_t); i \in \{1, \dots, 7\}\}. \quad (5)$$

Adversarial perturbation—Although the methods used to identify perturbation in images are not a perfect match for how humans perceive noise, L_p norms (with $p \in \{0, 2, \infty\}$) are commonly used since the early days of research on adversarial examples [8, 18, 44]. We use both L_2 and L_∞ norms for measuring the added perturbation. In terms of the used L_∞ perturbation budget, another large-scale study on adversarial transferability [51] uses $\epsilon_{[0,1]} \in \{0.1, 0.2, 0.3\}$, which approximately corresponds to $\epsilon_{[0,255]} \in \{25, 45, 67\}$ in discretized settings. We observed that using $\epsilon_{[0,255]} \geq 45$ leads to adversarial examples that come with large perturbation budgets. This means that these adversarial examples transfer from model-to-model trivially (i.e., for more than two-thirds of the attempts performed), but also that the exercised perturbation is typically easily visible to the bare eye. In light of this observation, we limit the perturbation on an L_∞ ball to 38 (i.e., $\epsilon_{[0,255]} = 38, \epsilon_{[0,1]} = 0.15$), thus ensuring that the perturbation is not visible to the bare eye. Further details on the calculation of L_p norms, as well as a comparison of perturbation visibility, can be found in the supplementary material.

For PGD, we perform the attack with 50 iterations and allow a perturbation budget of $\epsilon_{[0,1]} = 0.15$. For CW, we use $\kappa = 20$ (as suggested by [8]). We use targeted adversarial attacks, using a randomly targeted class that differs from the true class of the source image. In order to avoid cases where the image/target class combination is challenging, if an attack does not succeed under the allocated number of iterations, we select another class, and we perform the attack on the same image up to five times. At each iteration of the adversarial attack, we analyze whether or not the prediction for the image changed for the other six models (i.e., non-targeted transferability) and then select the adversarial examples with the smallest perturbation. By doing so, we aim at finding the least-required perturbation, as exercised

by both attacks, that is sufficient to convert a source image into an adversarial one.

Non-adversarial perturbation—In addition to the adversarial attacks, we also make use of commonly used image distortion techniques in order to measure the robustness of source images. For this analysis, we employ (1) uniform noise, (2) Gaussian noise, and (3) change in contrast to create “adversarial examples”, where all of these additive noises respect the L_∞ limit put in place for the PGD. Details on the usage of these operations can be found in the supplementary material.

4. Methodology for the source image analysis

In this section, we briefly explain the notation and methodology used for the analysis of source images in adversarial scenarios. We denote by $\hat{\mathbf{x}}^{(A):i \rightarrow j}$ an adversarial example that is created through the addition of adversarial perturbation with the attack $(A) \in \{\text{CW}, \text{PGD}\}$, calculated from the model θ_i , but that is misclassified by model θ_j , thus achieving adversarial transferability. We then denote the set of all adversarial examples that achieve adversarial transferability, created through the usage of source image \mathbf{x} , as follows:

$$\hat{\mathcal{X}}^{(A)} := \{\hat{\mathbf{x}}^{(A):i \rightarrow j} \mid i, j = 1, \dots, 7; i \neq j\}. \quad (6)$$

We measure the added perturbation with $L_{\{2, \infty\}}$ norms and denote the least amount of perturbation required to convert a source image into an adversarial example for a particular target model (j), regardless of which other model it is generated from, by:

$$d_p(\theta_j, \hat{\mathcal{X}}^{(A)}) = \min_{i \in \{1, \dots, 7\} \setminus \{j\}} \|\mathbf{x} - \hat{\mathbf{x}}^{(A):i \rightarrow j}\|_p, \quad (7)$$

where p denotes the selected norm. We also measure the minimum amount of perturbation required to convert a source image into an adversarial example for any model as:

$$D_p(\Theta, \hat{\mathcal{X}}^{(A)}) = \min_{j \in \{1, \dots, 7\}} d_p(\theta_j, \hat{\mathcal{X}}^{(A)}). \quad (8)$$

Another important benchmark is the transferability count of adversarial examples created from individual source images. Since we have seven models, and since we are only interested in model-to-model transferability, we count the successful model-to-model transfers for adversarial examples generated from a source image \mathbf{x} as follows:

$$T(\Theta, \hat{\mathcal{X}}^{(A)}, \mathbf{y}) = \sum_{i,j=1, i \neq j}^7 \mathbb{1}_{\{G(\theta_j, \hat{\mathbf{x}}^{(A):i \rightarrow j}) \neq \arg \max_t(\mathbf{y}_t)\}}. \quad (9)$$

For each source image, this transferability count $T(\Theta, \hat{\mathcal{X}}^{(A)}, \mathbf{y})$ can take a value between 0 and 42. In

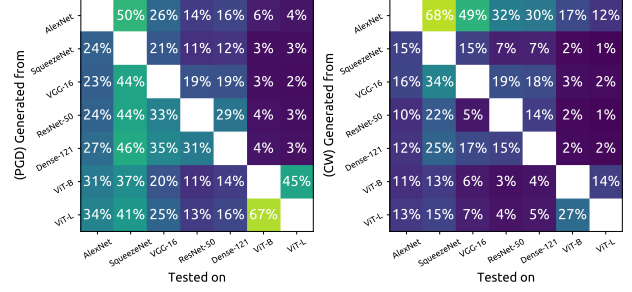


Figure 2: Proportion of source images that achieved adversarial transferability with the usage of PGD (left) and CW (right). Adversarial examples are generated from the models listed on the y -axis and are tested on the models listed on the x -axis.

this context, having zero model-to-model transferability means none of the adversarial examples generated from a particular source image achieved adversarial transferability and 42 means that the adversarial examples created from a source image achieved adversarial transferability in all model-to-model scenarios.

5. Experimental results

Through 1,598,100 adversarial attacks, we successfully create 294,368 adversarial examples that achieve adversarial transferability for at least one model-to-model scenario (excluding white-box cases). These adversarial examples originate from 15,580 source images, meaning that when the adversarial perturbation was exercised on the remaining 3,445 source images, their perturbed counterparts never became “adversarial” for the 42 model-to-model transferability scenarios evaluated in this study. We will refer to the set of 15,580 source images ($\sim 81\%$ of \mathbb{S}) that have an adversarial counterpart as

$$\mathbb{A} = \{\mathbf{x} \mid \hat{\mathcal{X}}^{(\text{CW}, \text{PGD}):i \rightarrow j} \neq \emptyset\}. \quad (10)$$

In the remainder of this paper, we provide and discuss experimental results for these 294,368 adversarial examples, as well as for the source images used to obtain them.

5.1. Model-to-model transferability

In Figure 2, we provide model-to-model transferability of adversarial examples generated with PGD (left) and CW (right). Specifically, this graph provides details for the source and target models of all 294,368 adversarial examples that achieved adversarial transferability. Although there are interesting observations to be made for model-to-model scenarios (these will be discussed later in Section 7), our primary goal is to identify the effects of source image selection on adversarial transferability.

Generated with	Uniform noise	1900	3772	1032	589	643	231	220
	Gaussian noise	3785	7027	2149	1187	1270	640	544
	Contrast change	2385	2314	620	437	326	219	222
		9.7%	19.3%	5.3%	3.0%	3.3%	1.2%	1.1%
		19.4%	35.9%	11.0%	6.1%	6.5%	3.3%	2.8%
		12.2%	11.8%	3.2%	2.2%	1.7%	1.1%	1.1%
		AlexNet	SqueezeNet	VGG-16	ResNet-50	Dense-121	ViT-B	ViT-L
		Tested on						

(a) Non-adversarial noise and source image transferability

(pCD) Generated from	AlexNet		76%	41%	23%	27%	10%	7%
	SqueezeNet	43%		36%	19%	21%	6%	5%
	VGG-16	41%	72%		33%	31%	5%	4%
	ResNet-50	43%	72%	52%		45%	6%	5%
	Dense-121	47%	73%	54%	47%		7%	5%
	ViT-B	50%	62%	33%	19%	23%		56%
	ViT-L	53%	65%	39%	23%	27%	77%	
		AlexNet	SqueezeNet	VGG-16	ResNet-50	Dense-121	ViT-B	ViT-L
Tested on								

(CW) Generated from	AlexNet		84%	65%	46%	44%	26%	18%
	SqueezeNet	27%		25%	12%	13%	3%	3%
	VGG-16	27%	53%		29%	28%	5%	4%
	ResNet-50	19%	38%	26%		23%	4%	3%
	Dense-121	21%	41%	27%	24%		4%	3%
	ViT-B	19%	24%	10%	6%	8%		21%
	ViT-L	22%	27%	12%	7%	9%	37%	
		AlexNet	SqueezeNet	VGG-16	ResNet-50	Dense-121	ViT-B	ViT-L
Tested on								

(b) Transferability of adversarial examples created with \mathbb{A}_n

(PCD) Generated from	AlexNet		28%	12%	4%	5%	3%	2%
	SqueezeNet	5%		7%	2%	3%	1%	1%
	VGG-16	4%	19%		7%	7%	1%	1%
	ResNet-50	5%	20%	17%		16%	1%	1%
	Dense-121	8%	23%	20%	17%		2%	1%
	ViT-B	14%	14%	8%	3%	4%		42%
	ViT-L	18%	19%	12%	4%	6%	74%	
		AlexNet	SqueezeNet	VGG-16	ResNet-50	Dense-121	ViT-B	ViT-L
Tested on								

(CW) Generated from	AlexNet		75%	46%	24%	22%	11%	6%
	SqueezeNet	4%		5%	2%	2%	0%	0%
	VGG-16	4%	18%		11%	9%	1%	0%
	ResNet-50	1%	7%	7%		6%	0%	0%
	Dense-121	2%	8%	8%	7%		0%	0%
	ViT-B	2%	2%	1%	1%	1%		10%
	ViT-L	3%	3%	2%	1%	1%	23%	
		AlexNet	SqueezeNet	VGG-16	ResNet-50	Dense-121	ViT-B	ViT-L
Tested on								

(c) Transferability of adversarial examples created with \mathbb{A}_p

Figure 3: (a) Number (proportion) of source images that have their classification changed with the usage of non-adversarial perturbation. (b) and (c) show model-to-model transferability of adversarial examples created with source images in \mathbb{A}_n and \mathbb{A}_p , respectively.

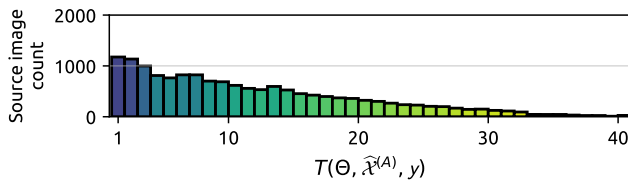


Figure 4: Histogram (count) of source images that achieved adversarial transferability.

In order to answer the question of whether or not adversarial transferability success can be influenced by the source image selection, let us continue with an unusual experiment. In Figure 3a, we reveal the number of source images that had their predictions changed for the models listed on the x -axis with the application of non-adversarial perturbations listed on the y -axis. Surprisingly, relying on common noise generation methods that do not require any special setup, we observe that a large portion of source images have their classification changed in a limited L_∞ ball setting. Specifically, 9,392 unique source images, corresponding to approximately 49% of the source images, become “adversarial examples” for at least one model with the introduction of non-adversarial noise.

Combining both experiments (Figure 2 and Figure 3) discussed thus far, let us divide \mathbb{A} into two sets \mathbb{A}_n and \mathbb{A}_p , where the former contains source images that had, at least once and for any model, their prediction changed with the application of non-adversarial noise (9,392 source images) and where the latter contains the remaining images (6,188 source images). According to this separation, we provide Figure 3b and Figure 3c, where we show model-to-model transferability of adversarial examples originating from source images in \mathbb{A}_n and \mathbb{A}_p , respectively. As it can be seen, even though (1) we use a large number of source images and (2) we know that it is possible to produce adversarial examples from source images residing in both \mathbb{A}_n and \mathbb{A}_p , we obtain completely differing outcomes for adversarial transferability success. We present detailed versions of all transferability matrices in the supplementary material.

The reason for the large discrepancy between the results presented in Figure 3b and Figure 3c is the fragility of a subset of source images. Compared to the other, non-fragile images, these fragile source images have their predictions easily changed for a large number of models, even when other conditions are held the same (e.g., attacks and models). In order to lay bare the fragility of these images, we perform an aggregate analysis of their transferability, leading to a histogram of $T(\Theta, \hat{x}^{(A)}, y)$ for all source images in \mathbb{A} , as shown in Figure 4. This histogram illustrates that almost half of the source images (9,680) achieve adversarial transferability up to 10 times. However, an intriguing observation can be made for the rightmost-side of this figure, where we can see that approximately 1,213 sources images achieve adversarial transferability more than 25 times. These fragile source images, which easily change predictions between models and which achieve unnaturally high model-to-model transferability compared to others, will be our main focus for the remainder of this paper.

5.2. Adversarial perturbation

Another important aspect of model-to-model adversarial transferability is how easy a source image becomes an

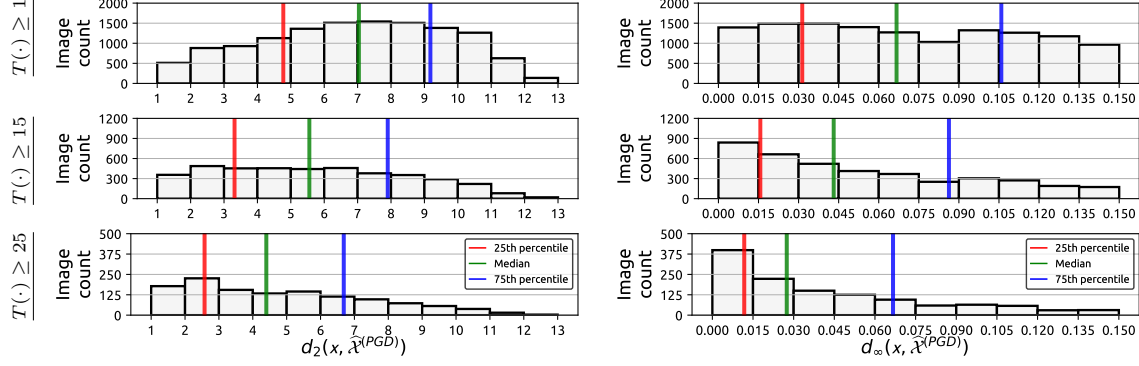


Figure 6: Source images that achieved adversarial transferability to ViT-B are selected based on the transferability counts with $T(\Theta, \hat{X}^{(\text{PGD})}, \mathbf{y}) \geq \{1, 15, 25\}$. The minimum amount of perturbation required for creating adversarial examples from these source images is histogrammed, measuring the perturbation using $d_p(\mathbf{x}, \hat{X}^{(\text{PGD})})$, with $p \in \{2, \infty\}$. The median perturbation, as well as the 25th and the 75th percentile, are provided in order to improve interpretability.

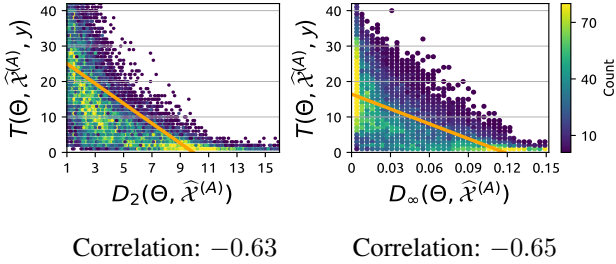


Figure 5: Scatter plot of $D_p(\Theta, \hat{X}^{(A)})$, the minimum amount of perturbation required for each source image, against adversarial transferability count $T(\Theta, \hat{X}^{(A)}, \mathbf{y})$, for $p = 2$ (left) and $p = \infty$ (right). The regression line is shown in orange.

adversarial example, since the robustness of adversarial defenses, as well as recently proposed models, are certified under an L_p norm perturbation. We first attempt at linking model-to-model adversarial transferability to the required perturbation to achieve this transferability for each source image. As such, we provide Figure 5, where we plot the adversarial transferability count for each source image, as obtained with $T(\Theta, \hat{X}^{(A)}, \mathbf{y})$, against the minimum required L_p perturbation to achieve adversarial transferability $D_{\{2, \infty\}}(\Theta, \hat{X}^{(A)})$. Here, we observe a mild negative correlation between added noise and transferability count, where the adversarial examples originating from source images that achieve higher transferability counts are also the ones that require less perturbation. These results hint that the fragile images we have identified do not only achieve high adversarial transferability, but that they also do so with smaller perturbation budgets.

In order to solidify these observation regarding perturbation and transferability, we part from an aggregate anal-

ysis to a more granular one and investigate the perturbations of adversarial examples that achieve transferability for each model individually. In Figure 6, we provide for ViT-B the smallest required $L_{\{2, \infty\}}$ perturbation for source images progressively filtered with $T(\Theta, \hat{X}, \mathbf{y}) \geq \{1, 10, 15\}$. Note that, as $T(\Theta, \hat{X}, \mathbf{y})$ increases, the distribution of the perturbation shifts towards zero, thus confirming our previous observations. These results indicate that source images that achieve high transferability counts are, most likely, also the ones that require less perturbation. Similar results can be observed for the other models. Detailed results are given in the supplementary material.

6. Source image suitability

Our experiments indicate that, while a certain portion of images never becomes adversarial examples, another portion of images can be easily turned into adversarial examples with a relatively small perturbation budget. Given the importance of research reproducibility, this leads to the question of how much variance can be observed when randomly sampling source images. In order to answer this question, we randomly sample 1,000 source images from \mathbb{S} (since this number seems to be the most commonly selected number in Figure 1), subsequently inspecting the adversarial examples generated from ViT-B and tested against ViT-L¹. We perform the aforementioned routine 10,000 times. As a result, in Table 1 (column \mathbb{S}), we provide the lowest, the highest, and the average transferability, as well as the $L_{\{2, \infty\}}$ perturbations. We observe that, while the average case closely matches the usage of all available source images provided in Figure 2, it is possible to have differences up to 12.5% in transferability, 1.01 in L_2 norm perturbation,

¹We observe similar results for all models used in this study. These results can be found in the supplementary material.

Table 1: The lowest, the highest, and the average transferability, as well as the $L_{\{2,\infty\}}$ perturbations are provided for adversarial examples created from randomly sampled 1,000 source images 10,000 times from the datasets provided in the second row. Statistics are provided based on adversarial examples that are created from ViT-B and tested on ViT-L.

			All images		Hard images		Easy (fragile) images		Filtered images	
			\mathbb{S}		$\mathbb{S}_{Q<10}$	$\mathbb{S}_{Q<25}$	$\mathbb{S}_{Q>90}$	$\mathbb{S}_{Q>75}$	$\mathbb{S} \setminus (\mathbb{S}_{Q<10} \cup \mathbb{S}_{Q>90})$	$\mathbb{S} \setminus (\mathbb{S}_{Q<25} \cup \mathbb{S}_{Q>75})$
Source images in set:			19,025		1,904	4,758	1,904	4,758	15,219	9,511
Transferability	PGD	Low	38.7%		23.2%	27.7%	69.2%	57.9%	38.8%	37.8%
		Avg	44.7%		27.5%	32.2%	72.8%	63.0%	43.5%	42.0%
		High	51.2%		30.8%	37.2%	77.4%	69.7%	47.3%	45.4%
	CW	Low	9.4%		2.0%	2.9%	40.1%	25.8%	10.1%	8.7%
		Avg	14.6%		3.8%	5.3%	44.2%	30.8%	13.5%	11.0%
		High	19.2%		5.4%	8.0%	49.7%	35.7%	17.7%	14.2%
Perturbation (L_2 / L_∞)	PGD	Low	6.00 / 0.05		6.79 / 0.07	6.67 / 0.06	4.68 / 0.03	5.31 / 0.04	6.27 / 0.06	6.41 / 0.06
		Avg	6.49 / 0.06		7.14 / 0.07	7.10 / 0.07	4.98 / 0.04	5.67 / 0.05	6.76 / 0.06	6.88 / 0.06
		High	7.01 / 0.07		7.54 / 0.08	7.49 / 0.08	5.26 / 0.04	6.01 / 0.05	6.98 / 0.07	7.14 / 0.07
	CW	Low	1.88 / 0.06		2.09 / 0.08	2.13 / 0.07	1.72 / 0.05	1.85 / 0.06	2.08 / 0.06	2.02 / 0.06
		Avg	2.25 / 0.08		2.56 / 0.09	2.53 / 0.08	1.85 / 0.05	2.05 / 0.06	2.42 / 0.07	2.40 / 0.07
		High	2.71 / 0.09		2.91 / 0.10	2.84 / 0.09	1.94 / 0.06	2.87 / 0.07	2.74 / 0.08	2.63 / 0.07

and 0.03 (i.e., $8/255$) in L_∞ norm perturbation between the lowest and the highest case. These results indicate that even with the usage of random sampling, it is indeed possible to have conflicting results, depending on the source images selected.

We showed in Section 5.1 that one way to identify fragile source images that are very easy for adversarial attacks is to perform a large-scale analysis of model-to-model transferability using all possible source images. However, such an approach is not scalable, unless an abundance of computational power is available, thus forcing us to investigate alternate methods for the identification of these atypical source images. An important piece of information we have for each source image is the vector of prediction probabilities obtained through the softmax function, $P(\theta, \mathbf{x}) = [e^{g(\theta, \mathbf{x})_c} / \sum_{k=1}^M e^{g(\theta, \mathbf{x})_k}]_{c \in \{1, \dots, M\}}$. The softmax output in conjunction with various error quantification methods has seen a significant use in recent research efforts on measuring the robustness and calibrated nature of DNNs [22]. Relying on the knowledge obtained from these studies, we use the following error quantification methods for evaluating the suitability of source images: (1) the error made for the correct class, as calculated by $1 - \max(P(\theta, \mathbf{x}))$, (2) mean absolute error (MAE), (3) mean squared error (MSE), (4) Wasserstein distance (WD), and (5) the ratio of probabilities: the second-largest to the largest one (Q). Details on the way the different errors are calculated can be found in the supplementary material.

In Table 2, we provide the correlation between (a) error measurement for the prediction of source images and (b) the properties of adversarial examples originating from those images (i.e., transferability and perturbation). Even though we use a large number of data points for this analysis, we still find a moderate correlation between multiple error estimates and adversarial properties. In particular, the

Table 2: Correlation between various estimates of errors in source image predictions and properties of adversarial examples created from those source images.

Error measurement	Correlation with		
	$T(\cdot)$	$\ \hat{\mathbf{x}} - \mathbf{x}\ _2$	$\ \hat{\mathbf{x}} - \mathbf{x}\ _\infty$
$Q(P(\theta, \mathbf{x}))$	0.52	-0.62	-0.63
$1 - \max(P(\theta, \mathbf{x}))$	0.50	-0.51	-0.53
$\text{MAE}(P(\theta, \mathbf{x}), \mathbf{y})$	0.48	-0.51	-0.51
$\text{MSE}(P(\theta, \mathbf{x}), \mathbf{y})$	0.53	-0.57	-0.57
$\text{WD}(P(\theta, \mathbf{x}), \mathbf{y})$	0.29	-0.33	-0.35

simple approach of $Q(\cdot)$ has the largest correlation when it comes to estimating perturbations, while having a comparably large correlation with transferability. In order to show this relation, in Figure 7, we scatter plot $Q(P(\theta, \mathbf{x}))$ against the L_p norm perturbations for each source image and the adversarial examples created from that source image. Based on Table 2 and Figure 7, we observe that, when $P(\theta, \mathbf{x})$ for a source image has its second-largest prediction closer to the largest one, adversarial examples originating from that source image are more likely to achieve adversarial transferability while requiring less perturbation.

In order to investigate the suitability of this measurement for approximating the properties of adversarial examples, we group source images according to the $Q(P(\theta, \mathbf{x}))$ value obtained. Specifically, we sort \mathbb{S} according to $Q(P(\theta, \mathbf{x}))$ and create subsets based on certain percentiles of $Q(\cdot)$. Doing so, in Table 1, we present the results for the same experimental routine described above (i.e., 1,000 source images sampled 10,000 times), but with a small difference: only the source images that have $Q(P(\theta, \mathbf{x}))$ larger than the 75th and 90th percentile ($\mathbb{S}_{Q>\{75,90\}}$), as well as less than the 10th and 25th percentile ($\mathbb{S}_{Q<\{10,25\}}$), are selected. We observe that source images with lower error estimates, as measured with $Q(P(\theta, \mathbf{x}))$, are harder to convert to adversarial examples, whereas the ones with higher

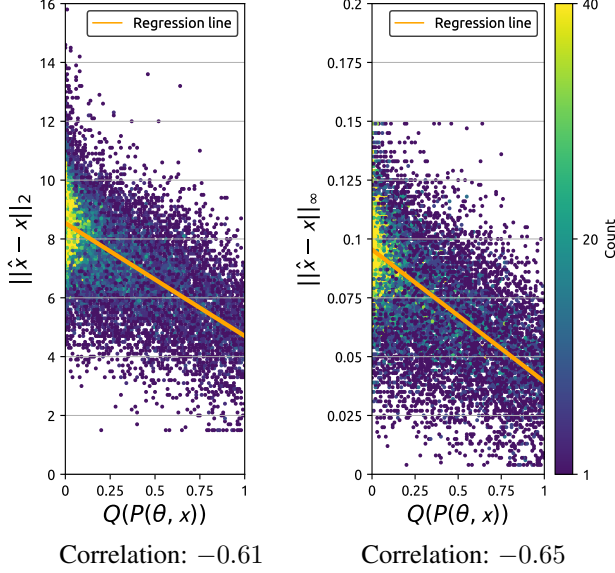


Figure 7: Measurements of $Q(P(\theta, \mathbf{x}))$ as obtained from all source images are plotted against the L_2 (left) and the L_∞ (right) perturbation norm of adversarial examples originating from the same source image. The regression line is shown in orange.

$Q(P(\theta, \mathbf{x}))$ estimates are much easier to convert. Not only that, the required amount of perturbation for creating adversarial examples also differs greatly between the lower and the upper-end of $Q(P(\theta, \mathbf{x}))$, with source images having a lower $Q(P(\theta, \mathbf{x}))$ requiring more perturbation, and vice versa. These results indicate that error estimates based on the prediction of source images can indeed be used as a proxy for the properties of adversarial examples originating from them.

Finally, in the two rightmost columns of Table 1, we present the results for adversarial properties obtained with source images filtered from both ends with $\mathbb{S} \setminus (\mathbb{S}_{Q < P} \cup \mathbb{S}_{Q > 100-P})$. As can be seen, we are able to reduce the difference between the highest and the lowest transferability from 12.5% to 7.6%, the difference in L_2 norm perturbation from 1.01 to 0.71, and the difference in L_∞ norm perturbation from 0.03 to 0.01, thus indicating a more stable experimentation closer to the average case. Furthermore when we filter the same number of images from both ends (e.g., $\mathbb{S} \setminus (\mathbb{S}_{Q < 10} \cup \mathbb{S}_{Q > 90})$), the average transferability goes down slightly compared to using all available source images, while the average amount of required perturbation goes up slightly. These results indicate that the usage of $Q(\cdot)$ is more reliable in identifying easy (fragile) source images than hard source images. As a result, we believe that further improvements on the way error measurements are performed can be made, and this with the usage of more complex analysis involving categories of source images.

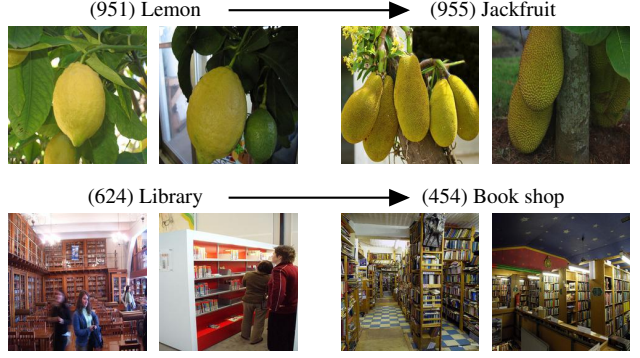


Figure 8: Adversarial examples on the left are misclassified as similar categories on the right by multiple models used in this study.

7. Conclusions and outlook

With the help of large-scale experiments, we exposed the fragility of a subset of source images, with the adversarial examples created from these fragile images achieving high adversarial transferability rates for a relatively small perturbation budget. We then took one of the first steps to identify the unusual source images that are either very hard or very easy to convert to adversarial examples in order to support high-quality experimentation.

Our experiments indicate that the adversarial examples created from ViT models easily transfer between each other, while the ones created from other models do not easily transfer to ViT models. We believe one of the reasons for this might be the pre-training of both models on ImageNet 21K [13, 15]. Given that transformer models recently achieved state-of-the-art results for vision tasks, in future work, we believe it is of high importance to analyze their adversarial robustness under various conditions and to discover the reasons for the observations explained above.

We noted that a large number of adversarial examples are misclassified as categories that are semantically close to the categories of their source images counterparts (see Figure 8). In this context, does a misclassification made for ImageNet, where the prediction is a semantically similar class (i.e., a dog breed is misclassified as another one), carry the same weight as a misclassification for an automated system in a self-driving car scenario (i.e., a human or a vehicle not identified)? As such, we believe an important item for future work is the analysis of misclassification categories, taking into account the semantic similarity of classes. We provide preliminary experiments on this topic in the supplementary material.

References

- [1] Martín Abadi, Ashish Agarwal, Paul Barham, Eugene Brevdo, Zhifeng Chen, Craig Citro, Greg S. Corrado,

- Andy Davis, Jeffrey Dean, Matthieu Devin, Sanjay Ghemawat, Ian Goodfellow, Andrew Harp, Geoffrey Irving, Michael Isard, Yangqing Jia, Rafal Jozefowicz, Lukasz Kaiser, Manjunath Kudlur, Josh Levenberg, Dandelion Mané, Rajat Monga, Sherry Moore, Derek Murray, Chris Olah, Mike Schuster, Jonathon Shlens, Benoit Steiner, Ilya Sutskever, Kunal Talwar, Paul Tucker, Vincent Vanhoucke, Vijay Vasudevan, Fernanda Viégas, Oriol Vinyals, Pete Warden, Martin Wattenberg, Martin Wicke, Yuan Yu, and Xiaoqiang Zheng. TensorFlow: Large-Scale Machine Learning on Heterogeneous Systems, 2015. 1
- [2] Anish Athalye and Nicholas Carlini. On The Robustness Of The CVPR 2018 White-Box Adversarial Example Defenses. *CoRR*, abs/1804.03286, 2018. 1, 3
- [3] Anish Athalye, Nicholas Carlini, and David Wagner. Obfuscated Gradients Give A False Sense Of Security: Circumventing Defenses To Adversarial Examples. *International Conference on Machine Learning*, 2018. 1
- [4] Shumeet Baluja and Ian Fischer. Adversarial Transformation Networks: Learning to Generate Adversarial Examples. *Proceedings of the AAAI Conference on Artificial Intelligence*, 2018. 2
- [5] Siddhant Bhambri, Sumanyu Muku, Avinash Tulasi, and Arun Balaji Buduru. A Survey of Black-Box Adversarial Attacks on Computer Vision Models. *arXiv*, pages arXiv–1912, 2019. 1
- [6] Wieland Brendel, Jonas Rauber, Matthias Kümmeler, Ivan Ustyuzhaninov, and Matthias Bethge. Accurate, Reliable and Fast Robustness Evaluation. In *Advances in Neural Information Processing Systems*, 2019. 2
- [7] Nicholas Carlini and David A. Wagner. Adversarial Examples Are Not Easily Detected: Bypassing Ten Detection Methods. *Proceedings of the 10th ACM Workshop on Artificial Intelligence and Security*, 2017. 1, 3
- [8] Nicholas Carlini and David A. Wagner. Towards Evaluating The Robustness of Neural Networks. *2017 IEEE Symposium on Security and Privacy*, 2017. 2, 3
- [9] Pin-Yu Chen, Yash Sharma, Huan Zhang, Jinfeng Yi, and Cho-Jui Hsieh. Ead: Elastic-Net Attacks to Deep Neural Networks via Adversarial Examples. *Proceedings of the AAAI Conference on Artificial Intelligence*, 2018. 2
- [10] Alesia Chernikova, Alina Oprea, Cristina Nita-Rotaru, and BaekGyu Kim. Are Self-Driving Cars Secure? Evasion Attacks Against Deep Neural Networks For Steering Angle Prediction. *IEEE Security and Privacy Workshops (SPW)*, 2019. 1
- [11] Francesco Croce and Matthias Hein. Sparse and Imperceivable Adversarial Attacks. In *Proceedings of the IEEE International Conference on Computer Vision*, 2019. 2
- [12] Francesco Croce and Matthias Hein. Provable robustness against all adversarial l_p -perturbations for $p \geq 1$. In *International Conference on Learning Representations*, 2020. 1
- [13] Jia Deng, Wei Dong, Richard Socher, Li-Jia Li, Kai Li, and Li Fei-Fei. Imagenet: A Large-Scale Hierarchical Image Database. In *Proceedings of the IEEE Conference on Computer Vision and Pattern Recognition*, 2009. 8
- [14] Yinpeng Dong, Qi-An Fu, Xiao Yang, Tianyu Pang, Hang Su, Zihao Xiao, and Jun Zhu. Benchmarking Adversarial Robustness on Image Classification. In *Proceedings of the IEEE Conference on Computer Vision and Pattern Recognition*, 2020. 2
- [15] Alexey Dosovitskiy, Lucas Beyer, Alexander Kolesnikov, Dirk Weissenborn, Xiaohua Zhai, Thomas Unterthiner, Mostafa Dehghani, Matthias Minderer, Georg Heigold, Sylvain Gelly, Jakob Uszkoreit, and Neil Houlsby. An Image is Worth 16x16 Words: Transformers for Image Recognition at Scale. In *International Conference on Learning Representations*, 2021. 3, 8
- [16] Chris Finlay, Aram-Alexandre Pooladian, and Adam Oberman. The LogBarrier Adversarial Attack: Making Effective use of Decision Boundary Information. In *Proceedings of the IEEE International Conference on Computer Vision*, 2019. 2
- [17] Samuel G Finlayson, Isaac S Kohane, and Andrew L Beam. Adversarial Attacks Against Medical Deep Learning Systems. *Science*, 363:1287–1289, 2019. 1
- [18] Justin Gilmer, Ryan P Adams, Ian Goodfellow, David Andersen, and George E Dahl. Motivating The Rules Of The Game For Adversarial Example Research. *CoRR*, abs/1807.06732, 2018. 2, 3, 23
- [19] Ian Goodfellow, Jonathon Shlens, and Christian Szegedy. Explaining and Harnessing Adversarial Examples. *International Conference on Learning Representations*, 2015. 2
- [20] Kathrin Grosse, Praveen Manoharan, Nicolas Papernot, Michael Backes, and Patrick McDaniel. On The (Statistical) Detection Of Adversarial Examples. *CoRR*, abs/1702.06280, 2017. 1
- [21] Chuan Guo, Jacob R Gardner, Yurong You, Andrew Gordon Wilson, and Kilian Q Weinberger. Simple Black-box Adversarial Attacks. *International Conference on Machine Learning*, 2019. 2

- [22] Chuan Guo, Geoff Pleiss, Yu Sun, and Kilian Q Weinberger. On Calibration of Modern Neural Networks. In *International Conference on Machine Learning*, 2017. 7
- [23] Kaiming He, Xiangyu Zhang, Shaoqing Ren, and Jian Sun. Deep Residual Learning For Image Recognition. In *Proceedings of the IEEE Conference on Computer Vision and Pattern Recognition*, 2016. 3
- [24] Shengyuan Hu, Tao Yu, Chuan Guo, Wei-Lun Chao, and Kilian Q Weinberger. A New Defense Against Adversarial Images: Turning a Weakness Into a Strength. In *Advances in Neural Information Processing Systems*, 2019. 2
- [25] Gao Huang, Zhuang Liu, Laurens Van Der Maaten, and Kilian Q Weinberger. Densely connected convolutional networks. In *Proceedings of the IEEE Conference on Computer Vision and Pattern Recognition*, 2017. 3
- [26] Forrest N Iandola, Song Han, Matthew W Moskewicz, Khalid Ashraf, William J Dally, and Kurt Keutzer. Squeezenet: Alexnet-level accuracy with 50x fewer parameters and 0.5 mb model size. *arXiv preprint arXiv:1602.07360*, 2016. 3
- [27] Andrew Ilyas, Logan Engstrom, Anish Athalye, and Jessy Lin. Black-box Adversarial Attacks with Limited Queries and Information. *International Conference on Machine Learning*, 2018. 2, 3
- [28] Eric Jones, Travis Oliphant, and Pearu Peterson. Scipy: Open Source Scientific Tools For Python, 2001. 1
- [29] Harini Kannan, Alexey Kurakin, and Ian Goodfellow. Adversarial Logit Pairing. *arXiv preprint arXiv:1803.06373*, 2018. 2
- [30] Danny Karmon, Daniel Zoran, and Yoav Goldberg. Lavan: Localized and Visible Adversarial Noise. *International Conference on Machine Learning*, 2018. 2
- [31] Jinkyu Koo, Michael Roth, and Saurabh Bagchi. Hawkeye: Adversarial Example Detector For Deep Neural Networks. *CoRR*, abs/1909.09938, 2019. 1
- [32] Alex Krizhevsky and Geoffrey Hinton. Learning Multiple Layers Of Features From Tiny Images. Technical report, Citeseer, 2009. 1
- [33] Alex Krizhevsky, Ilya Sutskever, and Geoffrey E Hinton. ImageNet classification with deep convolutional neural networks. In *Advances in Neural Information Processing Systems*, 2012. 1, 3
- [34] Alexey Kurakin, Ian Goodfellow, and Samy Bengio. Adversarial Examples In The Physical World. *Workshop Track, International Conference on Learning Representations*, 2016. 2
- [35] Yann LeCun, Léon Bottou, Yoshua Bengio, and Patrick Haffner. Gradient-Based Learning Applied To Document Recognition. *Proceedings of the IEEE*, 86(11):2278–2324, 1998. 1
- [36] Eden Levy, Yael Mathov, Ziv Katzir, Asaf Shabtai, and Yuval Elovici. Not all datasets are born equal: On heterogeneous data and adversarial examples. *arXiv preprint arXiv:2010.03180*, 2020. 1
- [37] Xin Li and Fuxin Li. Adversarial Examples Detection In Deep Networks With Convolutional Filter Statistics. In *Proceedings of the IEEE International Conference on Computer Vision*, 2017. 1
- [38] Xin Li and Fuxin Li. Adversarial Examples Detection in Deep Networks with Convolutional Filter Statistics. In *Proceedings of the IEEE International Conference on Computer Vision*, pages 5764–5772, 2017. 2
- [39] Fangzhou Liao, Ming Liang, Yinpeng Dong, Tianyu Pang, Xiaolin Hu, and Jun Zhu. Defense against adversarial attacks using high-level representation guided denoiser. In *Proceedings of the IEEE Conference on Computer Vision and Pattern Recognition*, pages 1778–1787, 2018. 2
- [40] Jan Hendrik Metzen, Mummadi Chaithanya Kumar, Thomas Brox, and Volker Fischer. Universal Adversarial Perturbations Against Semantic Image Segmentation. In *Proceedings of the IEEE International Conference on Computer Vision*, 2017. 1
- [41] Seyed-Mohsen Moosavi-Dezfooli, Alhussein Fawzi, Omar Fawzi, and Pascal Frossard. Universal Adversarial Perturbations. In *Proceedings of the IEEE Conference on Computer Vision and Pattern Recognition*, pages 1765–1773, 2017. 2
- [42] Seyed-Mohsen Moosavi-Dezfooli, Alhussein Fawzi, and Pascal Frossard. Deepfool: A Simple And Accurate Method To Fool Deep Neural Networks. In *Proceedings of the IEEE Conference on Computer Vision and Pattern Recognition*, 2016. 2
- [43] Utku Ozbulak, Manvel Gasparyan, Wesley De Neve, and Arnout Van Messem. Perturbation Analysis of Gradient-based Adversarial Attacks. *Pattern Recognition Letters*, 2020. 2
- [44] Nicolas Papernot, Patrick D. McDaniel, Xi Wu, Somesh Jha, and Ananthram Swami. Distillation As A Defense To Adversarial Perturbations Against Deep Neural Networks. *IEEE Symposium on Security and Privacy*, 2016. 3
- [45] Adam Paszke, Sam Gross, Soumith Chintala, Gregory Chanan, Edward Yang, Zachary DeVito, Zeming Lin, Alban Desmaison, Luca Antiga, and Adam Lerer. Automatic Differentiation in PyTorch. 2017. 1

- [46] Kevin Roth, Yannic Kilcher, and Thomas Hofmann. The Odds Are Odd: A Statistical Test For Detecting Adversarial Examples. In *International Conference on Machine Learning*, 2019. 1
- [47] A. Rozsa, E. M. Rudd, and T. E. Boult. Adversarial Diversity and Hard Positive Generation. In *Proceedings of the IEEE Conference on Computer Vision and Pattern Recognition Workshops*, 2016. 2
- [48] Olga Russakovsky, Jia Deng, Hao Su, Jonathan Krause, Sanjeev Satheesh, Sean Ma, Zhiheng Huang, Andrej Karpathy, Aditya Khosla, Michael Bernstein, Alexander C. Berg, and Li Fei-Fei. ImageNet Large Scale Visual Recognition Challenge. *International Journal of Computer Vision*, 115(3):211–252, 2015. 1
- [49] Ali Shahin Shamsabadi, Ricardo Sanchez-Matilla, and Andrea Cavallaro. Colorfool: Semantic Adversarial Colorization. In *Proceedings of the IEEE Conference on Computer Vision and Pattern Recognition*, 2020. 2
- [50] Karen Simonyan and Andrew Zisserman. Very Deep Convolutional Networks For Large-Scale Image Recognition. *International Conference on Learning Representations*, 2015. 3
- [51] Dong Su, Huan Zhang, Hongge Chen, Jinfeng Yi, Pin-Yu Chen, and Yupeng Gao. Is Robustness the Cost of Accuracy?—A Comprehensive Study on the Robustness of 18 Deep Image Classification Models. In *Proceedings of the European Conference on Computer Vision*, pages 631–648, 2018. 2, 3
- [52] Lu Sun, Mingtian Tan, and Zhe Zhou. A Survey of Practical Adversarial Example Attacks. *Cybersecurity*, 1(1):9, 2018. 1
- [53] Christian Szegedy, Wojciech Zaremba, Ilya Sutskever, Joan Bruna, Dumitru Erhan, Ian Goodfellow, and Rob Fergus. Intriguing Properties Of Neural Networks. *International Conference on Learning Representations*, 2014. 1, 2
- [54] Florian Tramer, Nicholas Carlini, Wieland Brendel, and Aleksander Madry. On Adaptive Attacks to Adversarial Example Defenses. *Advances in Neural Information Processing Systems*, 2020. 1, 2
- [55] Chun-Chen Tu, Paishun Ting, Pin-Yu Chen, Sijia Liu, Huan Zhang, Jinfeng Yi, Cho-Jui Hsieh, and Shin-Ming Cheng. Autozoom: Autoencoder-based Zeroth Order Optimization Method for Attacking Black-Box Neural Networks. In *Proceedings of the AAAI Conference on Artificial Intelligence*, 2019. 3
- [56] Vaswani, Ashish and Shazeer, Noam and Parmar, Niki and Uszkoreit, Jakob and Jones, Llion and Gomez, Aidan N and Kaiser, Łukasz and Polosukhin, Illia. Attention is All you Need. In *Advances in Neural Information Processing Systems*, 2017. 1
- [57] Ke Wang, Guangyu Wang, Ning Chen, and Ting Chen. How Robust Is Your Automatic Diagnosis Model? In *2019 IEEE International Conference on Bioinformatics and Biomedicine*, 2019. 1
- [58] Dongxian Wu, Yisen Wang, Shu-Tao Xia, James Bailey, and Xingjun Ma. Skip Connections Matter: On the Transferability of Adversarial Examples Generated with ResNets. In *International Conference on Learning Representations*, 2020. 2
- [59] Cihang Xie, Mingxing Tan, Boqing Gong, Jiang Wang, Alan L Yuille, and Quoc V Le. Adversarial Examples Improve Image Recognition. In *Proceedings of the IEEE Conference on Computer Vision and Pattern Recognition*, 2020. 2
- [60] Cihang Xie, Jianyu Wang, Zhishuai Zhang, Zhou Ren, and Alan Yuille. Mitigating Adversarial Effects Through Randomization. *International Conference on Learning Representations*, 2018. 2
- [61] Kaidi Xu, Sijia Liu, Pu Zhao, Pin-Yu Chen, Huan Zhang, Quanfu Fan, Deniz Erdogmus, Yanzhi Wang, and Xue Lin. Structured Adversarial Attack: Towards General Implementation and Better Interpretability. *International Conference on Learning Representations*, 2019. 2
- [62] Ziang Yan, Yiwen Guo, and Changshui Zhang. Deep Defense: Training DNNs with Improved Adversarial Robustness. In *Advances in Neural Information Processing Systems*, 2018. 2
- [63] X. Yuan, P. He, Q. Zhu, R. Rana Bhat, and X. Li. Adversarial Examples: Attacks And Defenses For Deep Learning. *IEEE Transactions on Neural Networks and Learning Systems*, 30:2805–2824, 2019. 1
- [64] Yuchen Zhang and Percy Liang. Defending against Whitebox Adversarial Attacks via Randomized Discretization. In *The 22nd International Conference on Artificial Intelligence and Statistics*, pages 684–693, 2019. 2
- [65] Zhengyu Zhao, Zhuoran Liu, and Martha Larson. Towards Large yet Imperceptible Adversarial Image Perturbations with Perceptual Color Distance. In *Proceedings of the IEEE Conference on Computer Vision and Pattern Recognition*, pages 1039–1048, 2020. 2

A. L_p norms and perturbation visibility

Although we guarantee the discretization property, in order to maintain comparability with the literature, the perturbation amounts reported in the main text (both L_2 and L_∞) are calculated based on the assumption that pixel values lie in $[0, 1]$. Based on this, we calculate the L_2 and L_∞ distance between two vectors with size $k = 3 \times 224 \times 224$ (channel \times height \times width) images as follows:

$$L_2(\mathbf{x}, \hat{\mathbf{x}}) = \|\mathbf{x} - \hat{\mathbf{x}}\|_2, \quad (11)$$

$$L_\infty(\mathbf{x}, \hat{\mathbf{x}}) = \max(|\mathbf{x} - \hat{\mathbf{x}}|), \quad (12)$$

where \mathbf{x} and $\hat{\mathbf{x}}$ represent an initial image and its adversarial counterpart, respectively. In Figure 9, we provide a number of qualitative examples for measuring the perturbation visibility.

B. Non-adversarial perturbations

In the main text, we compare the adversarial transferability of images modified with adversarial perturbation with that of images changed with non-adversarial noise. The different types of non-adversarial noise we employ are (1) uniform noise, (2) normal noise, and (3) change in the contrast. For the aforementioned noises we initialize a vector $\mathbf{p} = \mathbf{0} \in \mathbb{R}^k$ which has the same size as the input and fill its values as described below, with all non-adversarial perturbation generation methods respecting the L_∞ perturbation limit set for the PGD with the usage of $\Pi_{\epsilon=38}$.

Uniform noise—Similar to the employed usage of the Projected Gradient Descent (PGD) attack, we use an iterative approach for the application of the uniform noise. As such, each of the elements of \mathbf{p} is sampled from a uniform distribution $\mathcal{U}[-1, 1]$, but instead of using the values themselves we use their signature and apply the perturbation as follows:

$$[\hat{\mathbf{x}}]_{n+1} = \Pi_\epsilon([\hat{\mathbf{x}}]_n + [\mathbf{p}]_n), [\mathbf{p}]_n \sim \text{sign}(\mathcal{U}[-1, 1]). \quad (13)$$

with $[\hat{\mathbf{x}}]_1 = \mathbf{x}$. Similar to the usage of PGD, if the “adversarial example” created this way does not achieve model-to-model transferability, we perform the same operation four additional times.

Gaussian noise—Instead of an iterative approach, we follow a different methodology for the application of the Gaussian noise. We sample only one noise vector with every element of this vector originating from a Gaussian distribution with zero mean and standard deviation 10. We then apply this noise vector to the data point at hand as follows:

$$\hat{\mathbf{x}} = \Pi_\epsilon(\mathbf{x} + \mathbf{p}), \mathbf{p}_k \sim \mathcal{N}(0, 10^2). \quad (14)$$

If the image at hand does not achieve adversarial transferability, we perform the same operation up to ten times with newly sampled values from the same normal distribution.

Contrast change—Contrast change for the image domain means that all pixel values are modified with the same value. For this approach, we evaluate all possible values within the allowed L_∞ limit, creating a set of adversarial examples originating from an input as follows:

$$\hat{\mathcal{X}} := \{\hat{\mathbf{x}}_b \mid \hat{\mathbf{x}}_b = \mathbf{x} + \mathbf{1} * b, b \in \{-38, \dots, 38\}\}. \quad (15)$$

C. Detailed transferability graphs

In Figure 10 and Figure 11, we provide the model-to-model transferability figures presented in Figure 2 and Figure 3 in the main text but in a higher resolution and with more details.

D. Required perturbation for adversarial transferability

In Figure 6 of the main text we provided, for ViT-B, the $L_{\{2, \infty\}}$ norms of perturbations applied on images to achieve adversarial transferability. In Figure 12 to Figure 18 we provide the same results for the other models.

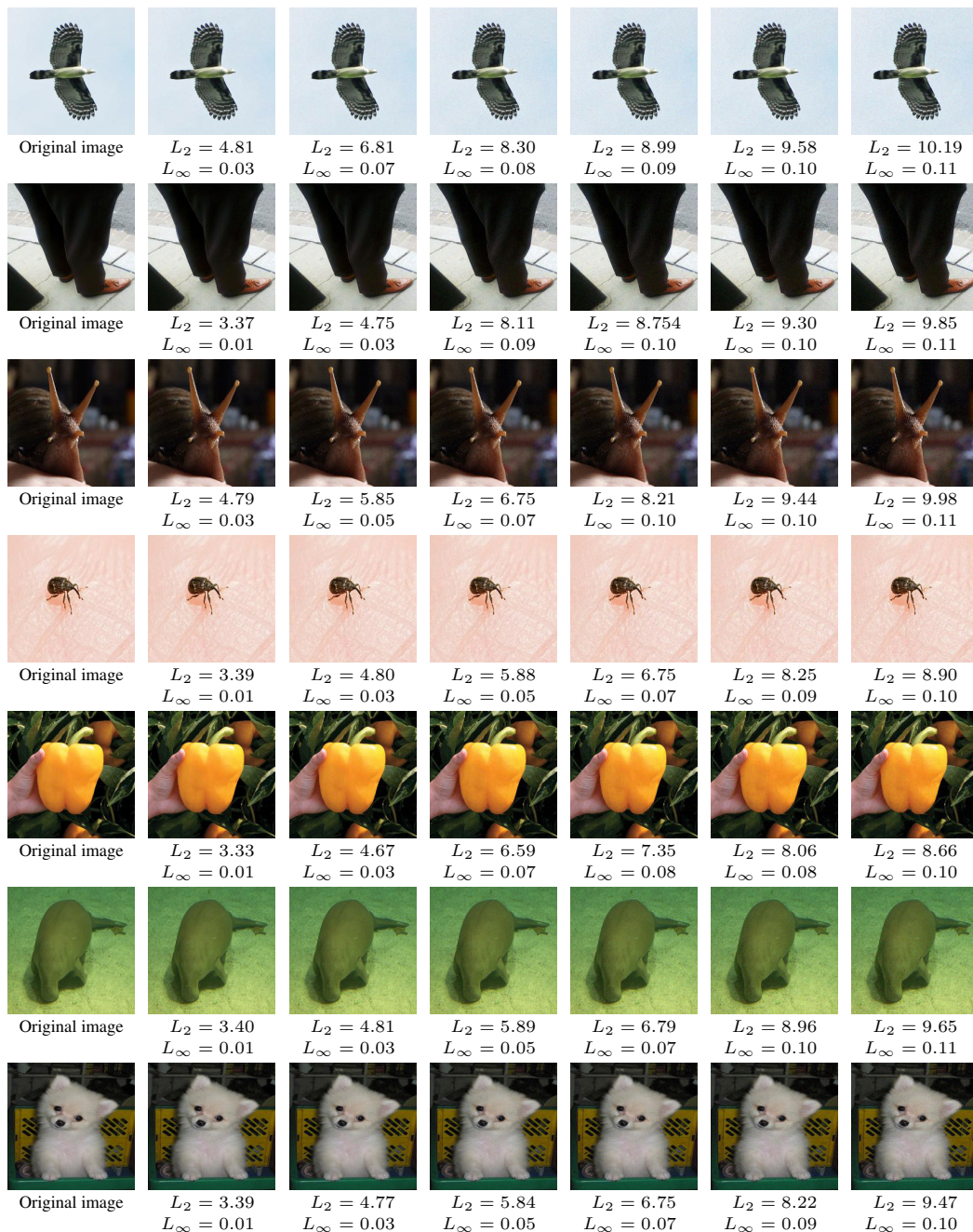


Figure 9: Application of adversarial perturbations on images.

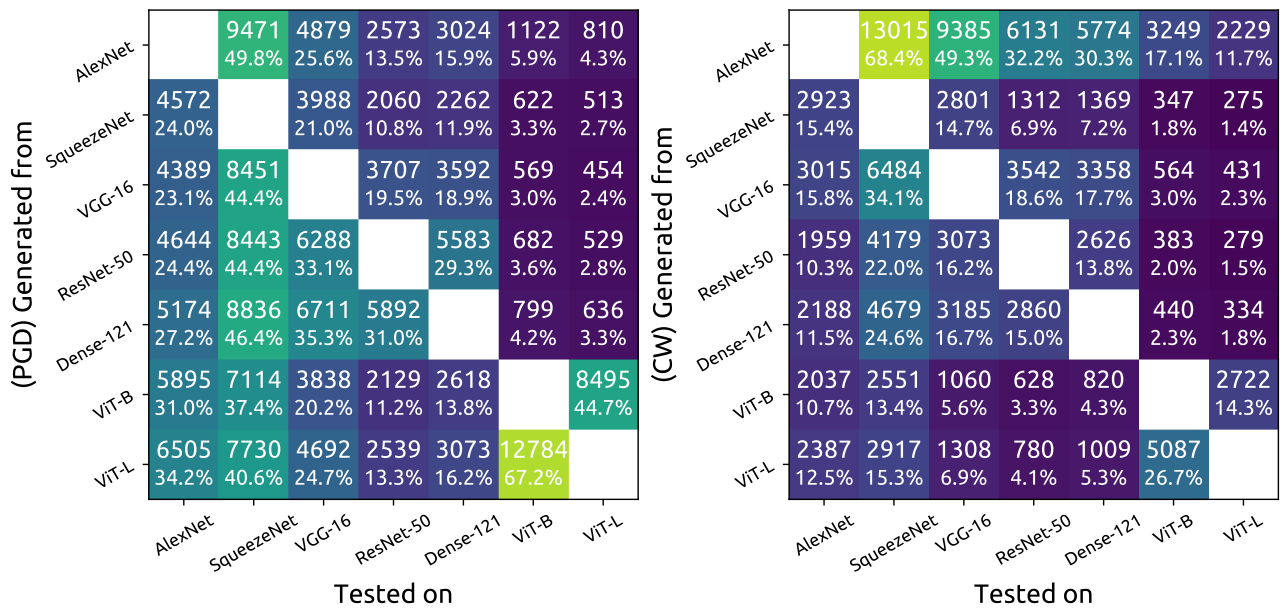


Figure 10: Proportion of source images that achieved adversarial transferability with the usage of PGD (left) and CW (right). Adversarial examples are generated from the models listed on the y -axis and are tested on the models listed on the x -axis.

Generated with	Uniform noise	1900 9.7%	3772 19.3%	1032 5.3%	589 3.0%	643 3.3%	231 1.2%	220 1.1%
	Gaussian noise	3785 19.4%	7027 35.9%	2149 11.0%	1187 6.1%	1270 6.5%	640 3.3%	544 2.8%
	Contrast change	2385 12.2%	2314 11.8%	620 3.2%	437 2.2%	326 1.7%	219 1.1%	222 1.1%
		AlexNet	SqueezeNet	VGG-16	ResNet-50	Dense-121	ViT-B	ViT-L
		Tested on						

(a) Non-adversarial noise and source image transferability

(PGD) Generated from	AlexNet		7556 75.4%	4092 40.8%	2318 23.1%	2670 26.6%	1012 10.1%	731 7.3%
	SqueezeNet	4250 42.4%		3537 35.3%	1931 19.3%	2068 20.6%	604 6.0%	495 4.9%
	VGG-16	4106 40.9%	7165 71.5%		3248 32.4%	3128 31.2%	542 5.4%	436 4.3%
	ResNet-50	4297 42.9%	7115 71.0%	5162 51.5%		4509 45.0%	646 6.4%	504 5.0%
	Dense-121	4633 46.2%	7253 72.3%	5371 53.6%	4727 47.1%		742 7.4%	594 5.9%
	ViT-B	4968 49.5%	6151 61.3%	3282 32.7%	1936 19.3%	2314 23.1%		5684 56.7%
	ViT-L	5309 52.9%	6447 64.3%	3881 38.7%	2253 22.5%	2685 26.8%	7768 77.5%	
		AlexNet	SqueezeNet	VGG-16	ResNet-50	Dense-121	ViT-B	ViT-L
		Tested on						

(CW) Generated from	AlexNet		8398 83.8%	6538 65.2%	4655 46.4%	4439 44.3%	2591 25.8%	1834 18.3%
	SqueezeNet	2688 26.8%		2468 24.6%	1213 12.1%	1259 12.6%	336 3.4%	263 2.6%
	VGG-16	2754 27.5%	5342 53.3%		2868 28.6%	2808 28.0%	528 5.3%	409 4.1%
	ResNet-50	1876 18.7%	3776 37.7%	2637 26.3%		2279 22.7%	364 3.6%	266 2.7%
	Dense-121	2075 20.7%	4161 41.5%	2685 26.8%	2431 24.2%		420 4.2%	322 3.2%
	ViT-B	1910 19.0%	2404 24.0%	983 9.8%	595 5.9%	767 7.6%		2108 21.0%
	ViT-L	2208 22.0%	2727 27.2%	1198 11.9%	727 7.3%	936 9.3%	3679 36.7%	
		AlexNet	SqueezeNet	VGG-16	ResNet-50	Dense-121	ViT-B	ViT-L
		Tested on						

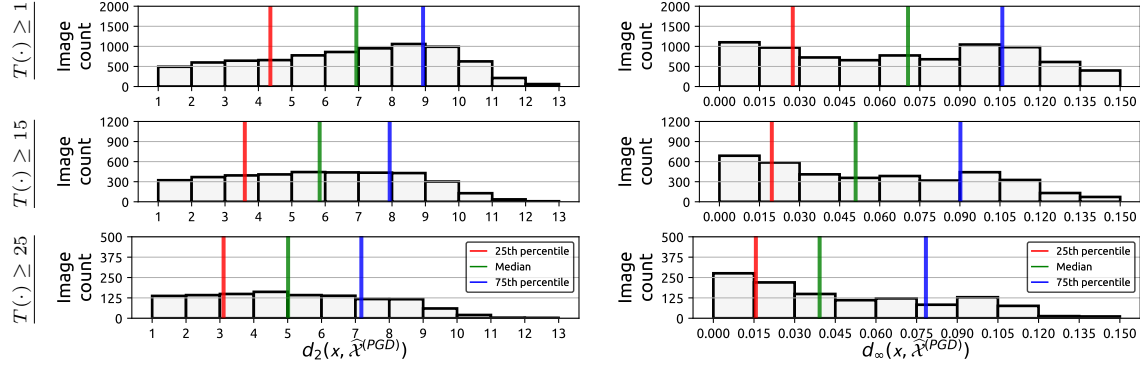
(b) Transferability of adversarial examples created with \mathbb{A}_n

(PGD) Generated from	AlexNet		1915 28.0%	787 11.5%	255 3.7%	354 5.2%	110 1.6%	79 1.2%
	SqueezeNet	322 4.7%		451 6.6%	129 1.9%	194 2.8%	18 0.3%	18 0.3%
	VGG-16	283 4.1%	1286 18.8%		459 6.7%	464 6.8%	27 0.4%	18 0.3%
	ResNet-50	347 5.1%	1328 19.4%	1126 16.4%		1074 15.7%	36 0.5%	25 0.4%
	Dense-121	541 7.9%	1583 23.1%	1340 19.6%	1165 17.0%		57 0.8%	42 0.6%
	ViT-B	927 13.5%	963 14.1%	556 8.1%	193 2.8%	304 4.4%		2811 41.1%
	ViT-L	1196 17.5%	1283 18.7%	811 11.8%	286 4.2%	388 5.7%	5016 73.3%	
		AlexNet	SqueezeNet	VGG-16	ResNet-50	Dense-121	ViT-B	ViT-L
		Tested on						

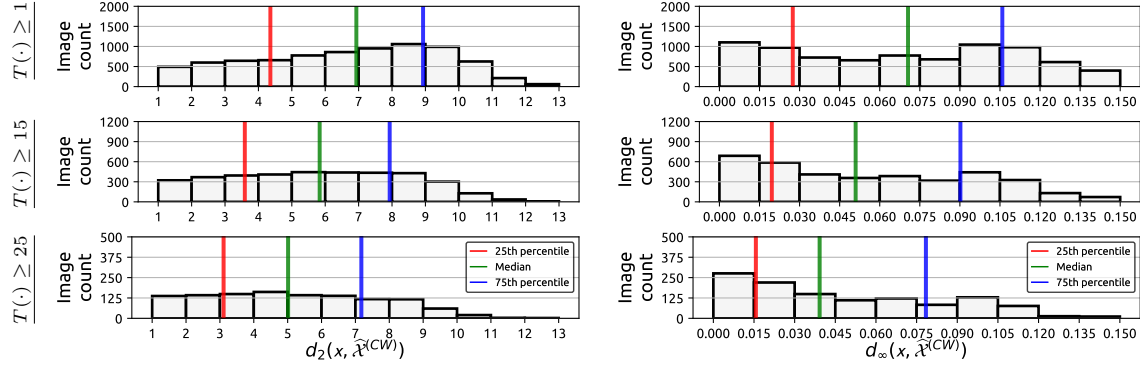
(CW) Generated from	AlexNet		4617 74.6%	2847 46.0%	1476 23.9%	1335 21.6%	658 10.6%	395 6.4%
	SqueezeNet	235 3.8%		333 5.4%	99 1.6%	110 1.8%	11 0.2%	12 0.2%
	VGG-16	261 4.2%	1142 18.5%		674 10.9%	550 8.9%	36 0.6%	22 0.4%
	ResNet-50	83 1.3%	403 6.5%	436 7.0%		347 5.6%	19 0.3%	13 0.2%
	Dense-121	113 1.8%	518 8.4%	500 8.1%	429 6.9%		20 0.3%	12 0.2%
	ViT-B	127 2.1%	147 2.4%	77 1.2%	33 0.5%	53 0.9%		614 9.9%
	ViT-L	179 2.9%	190 3.1%	110 1.8%	53 0.9%	73 1.2%	1408 22.8%	
		AlexNet	SqueezeNet	VGG-16	ResNet-50	Dense-121	ViT-B	ViT-L
		Tested on						

(c) Transferability of adversarial examples created with \mathbb{A}_p

Figure 11: (a) Number (proportion) of source images that have their classification changed with the usage of non-adversarial perturbation. (b) and (c) show model-to-model transferability of adversarial examples created with source images in \mathbb{A}_n and \mathbb{A}_p , respectively.

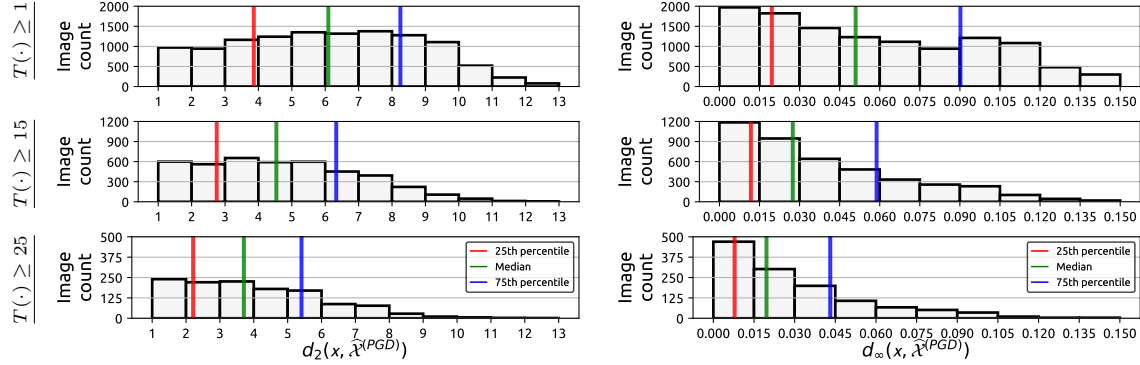


(a) Adversarial examples transferred to **AlexNet** with PGD.

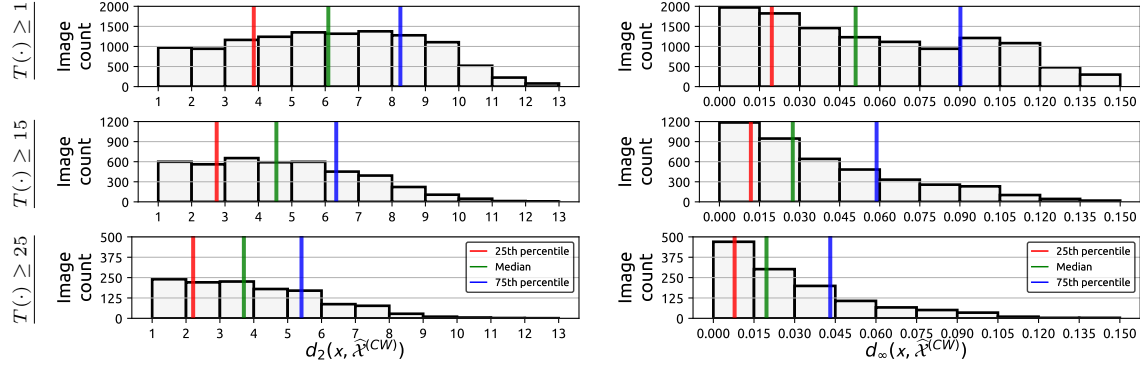


(b) Adversarial examples transferred to **AlexNet** with CW.

Figure 12: Source images that achieved adversarial transferability to **AlexNet** are selected based on the transferability counts with $T(\Theta, \hat{\mathcal{X}}^{(A)}, \mathbf{y}) \geq \{1, 15, 25\}$. The minimum amount of perturbation required for creating adversarial examples from these source images is histogrammed, measuring the perturbation using $d_p(\mathbf{x}, \hat{\mathcal{X}}^{(A)})$, with $p \in \{2, \infty\}$. The median perturbation, as well as the 25th and the 75th percentile, are provided in order to improve interpretability.

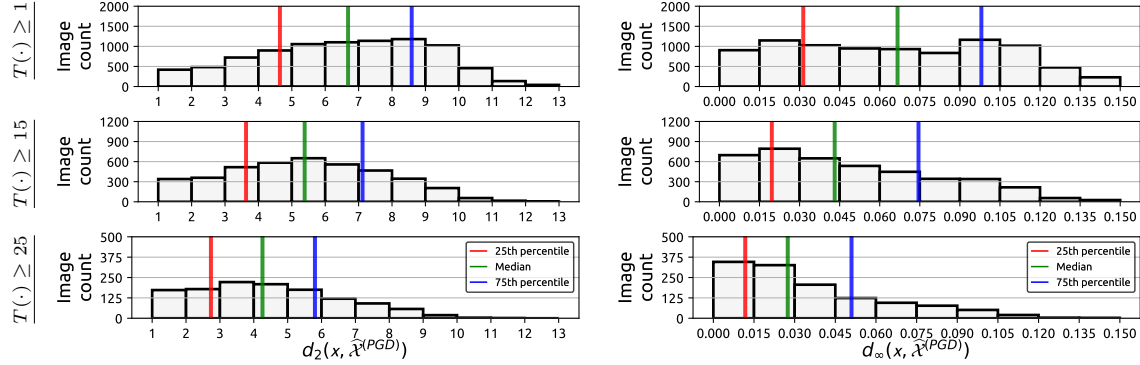


(a) Adversarial examples transferred to **SqueezeNet** with **PGD**.

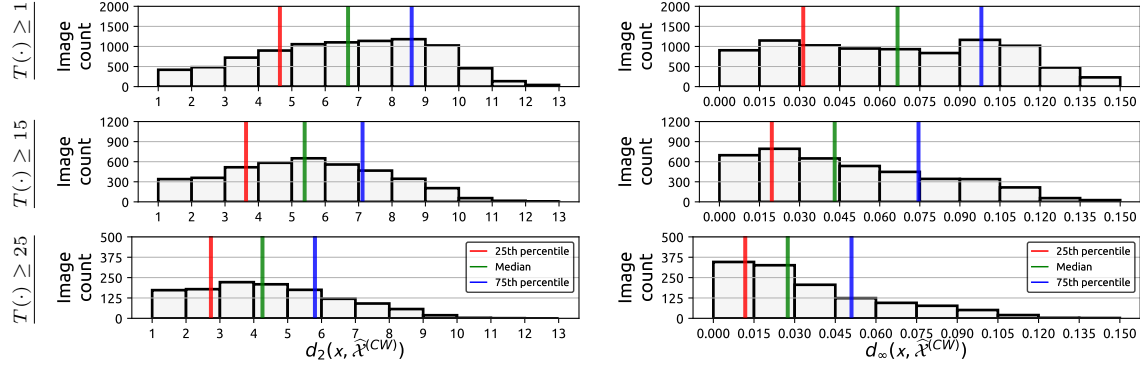


(b) Adversarial examples transferred to **SqueezeNet** with **CW**.

Figure 13: Source images that achieved adversarial transferability to **SqueezeNet** are selected based on the transferability counts with $T(\Theta, \hat{\mathcal{X}}^{(A)}, \mathbf{y}) \geq \{1, 15, 25\}$. The minimum amount of perturbation required for creating adversarial examples from these source images is histogrammed, measuring the perturbation using $d_p(x, \hat{\mathcal{X}}^{(A)})$, with $p \in \{2, \infty\}$. The median perturbation, as well as the 25th and the 75th percentile, are provided in order to improve interpretability.

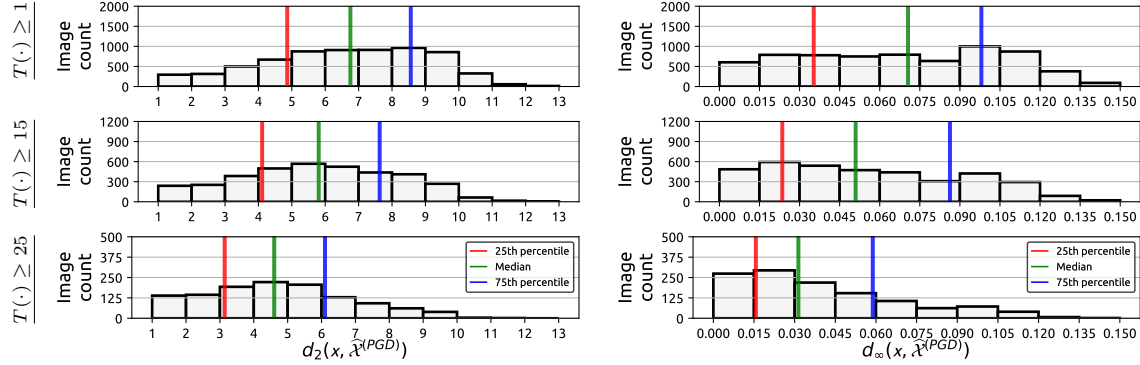


(a) Adversarial examples transferred to **VGG-16** with **PGD**.

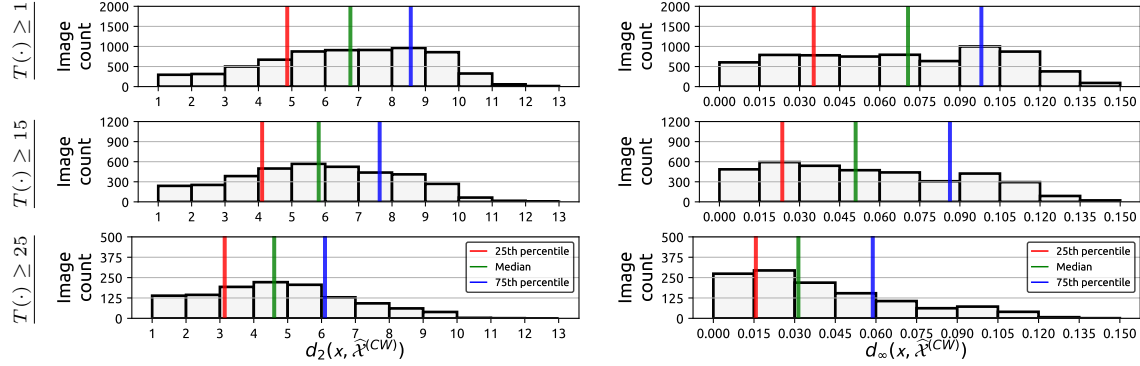


(b) Adversarial examples transferred to **VGG-16** with **CW**.

Figure 14: Source images that achieved adversarial transferability to **VGG-16** are selected based on the transferability counts with $T(\Theta, \hat{\mathcal{X}}^{(A)}, \mathbf{y}) \geq \{1, 15, 25\}$. The minimum amount of perturbation required for creating adversarial examples from these source images is histogrammed, measuring the perturbation using $d_p(\mathbf{x}, \hat{\mathcal{X}}^{(A)})$, with $p \in \{2, \infty\}$. The median perturbation, as well as the 25th and the 75th percentile, are provided in order to improve interpretability.

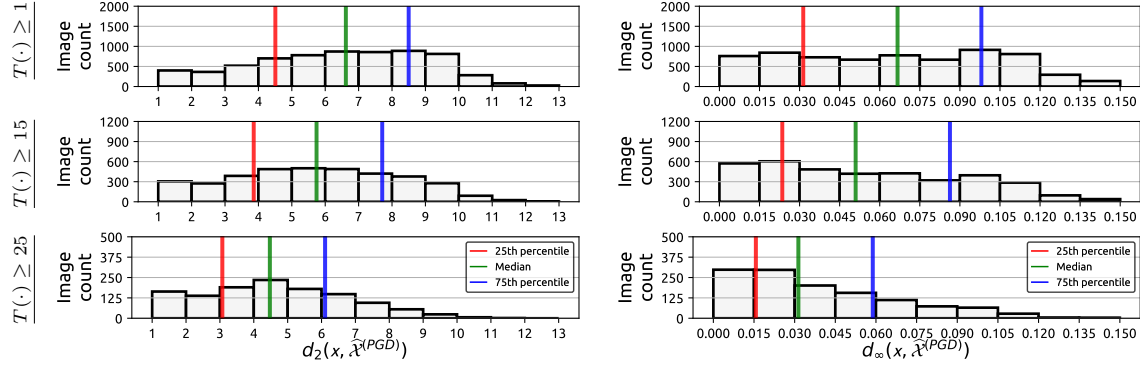


(a) Adversarial examples transferred to **ResNet-50** with **PGD**.

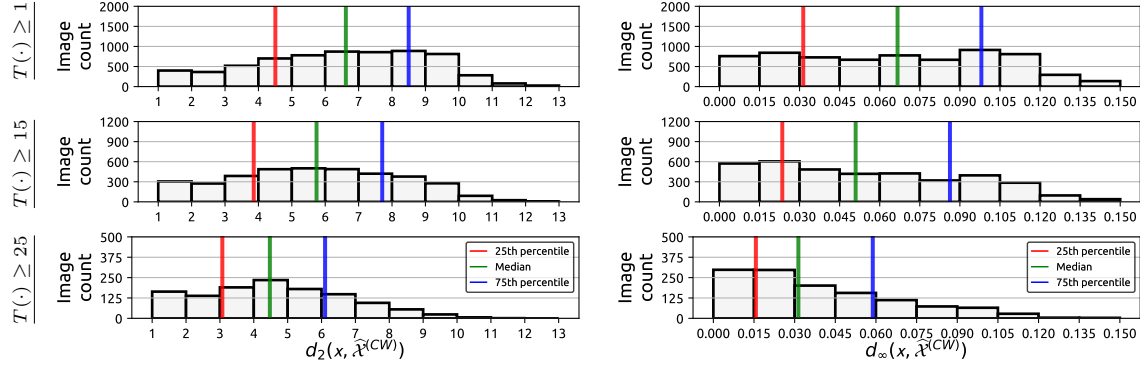


(b) Adversarial examples transferred to **ResNet-50** with **CW**.

Figure 15: Source images that achieved adversarial transferability to **ResNet-50** are selected based on the transferability counts with $T(\Theta, \hat{\mathcal{X}}^{(A)}, \mathbf{y}) \geq \{1, 15, 25\}$. The minimum amount of perturbation required for creating adversarial examples from these source images is histogrammed, measuring the perturbation using $d_p(x, \hat{\mathcal{X}}^{(A)})$, with $p \in \{2, \infty\}$. The median perturbation, as well as the 25th and the 75th percentile, are provided in order to improve interpretability.

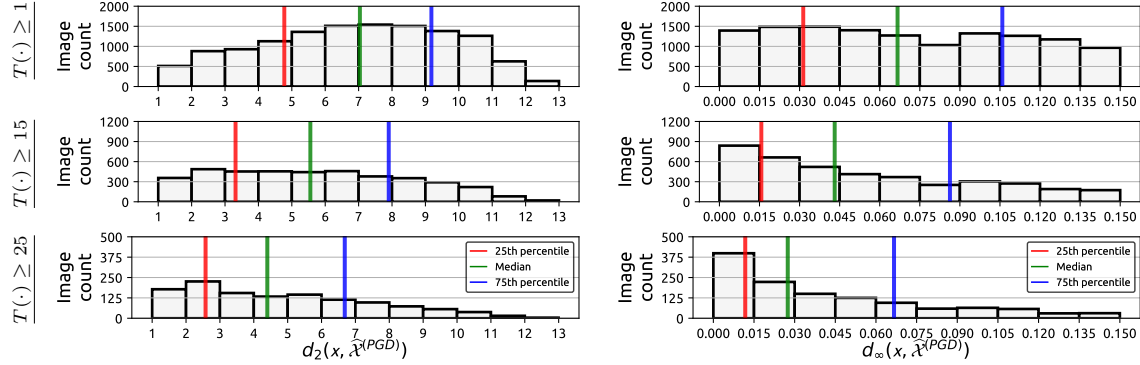


(a) Adversarial examples transferred to **DenseNet-121** with PGD.

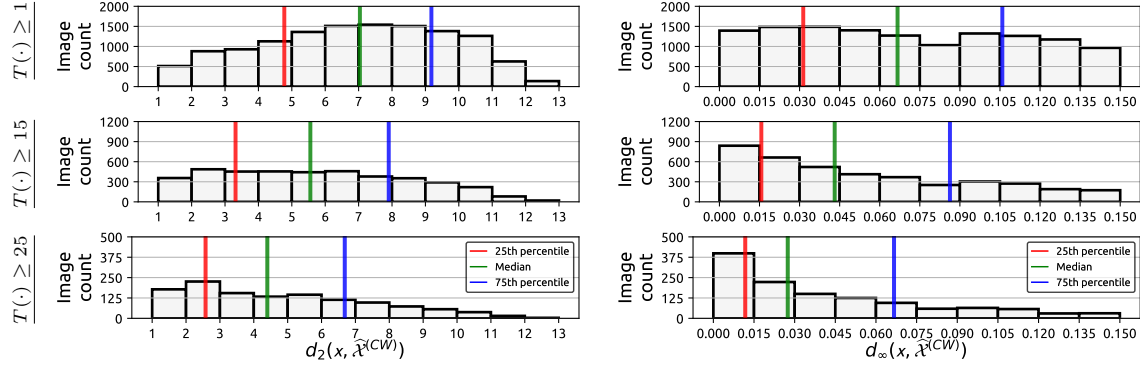


(b) Adversarial examples transferred to **DenseNet-121** with CW.

Figure 16: Source images that achieved adversarial transferability to **DenseNet-121** are selected based on the transferability counts with $T(\Theta, \hat{\mathcal{X}}^{(A)}, \mathbf{y}) \geq \{1, 15, 25\}$. The minimum amount of perturbation required for creating adversarial examples from these source images is histogrammed, measuring the perturbation using $d_p(x, \hat{\mathcal{X}}^{(A)})$, with $p \in \{2, \infty\}$. The median perturbation, as well as the 25th and the 75th percentile, are provided in order to improve interpretability.

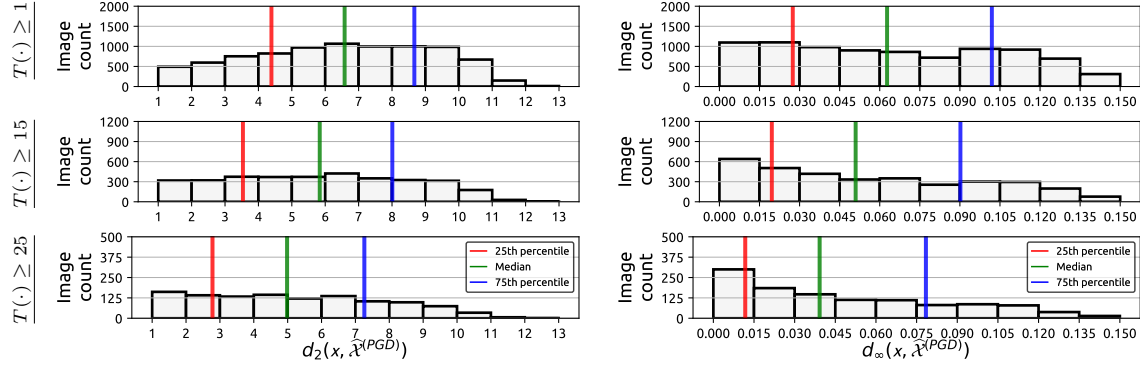


(a) Adversarial examples transferred to **ViT-B** with **PGD**.

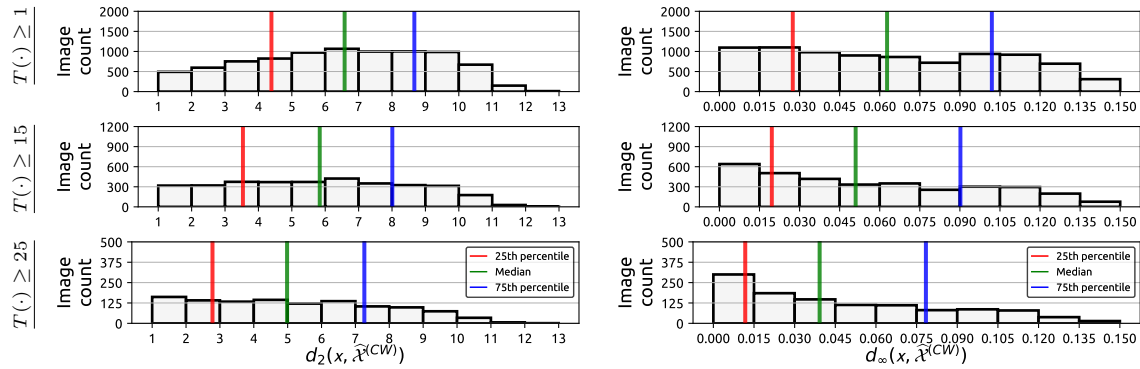


(b) Adversarial examples transferred to **ViT-B** with **CW**.

Figure 17: Source images that achieved adversarial transferability to **ViT-B** are selected based on the transferability counts with $T(\Theta, \hat{\mathcal{X}}^{(A)}, \mathbf{y}) \geq \{1, 15, 25\}$. The minimum amount of perturbation required for creating adversarial examples from these source images is histogrammed, measuring the perturbation using $d_p(\mathbf{x}, \hat{\mathcal{X}}^{(A)})$, with $p \in \{2, \infty\}$. The median perturbation, as well as the 25th and the 75th percentile, are provided in order to improve interpretability.



(a) Adversarial examples transferred to ViT-L with PGD.



(b) Adversarial examples transferred to ViT-L with CW.

Figure 18: Source images that achieved adversarial transferability to ViT-L are selected based on the transferability counts with $T(\Theta, \hat{\mathcal{X}}^{(A)}, \mathbf{y}) \geq \{1, 15, 25\}$. The minimum amount of perturbation required for creating adversarial examples from these source images is histogrammed, measuring the perturbation using $d_p(\mathbf{x}, \hat{\mathcal{X}}^{(A)})$, with $p \in \{2, \infty\}$. The median perturbation, as well as the 25th and the 75th percentile, are provided in order to improve interpretability.

E. Error estimates

In the main text we briefly noted the usage of a number of error estimates in order to measure mistakes made in the prediction of source images. For \mathbf{y} the true probabilistic categorical distribution associated with a data point \mathbf{x} , assume that $c = \arg \max(\mathbf{y})$ is the true class and $\hat{\mathbf{y}} = P(\theta, \mathbf{x})$ is the prediction obtained with a model described by its parameters θ . The error estimates are then defined, in the context of ImageNet, as:

$$\text{MAE}(\hat{\mathbf{y}}, \mathbf{y}) = \frac{1}{1,000} \sum_{k=0}^{1,000} |y_k - \hat{y}_k|, \quad (16)$$

$$\text{MSE}(\hat{\mathbf{y}}, \mathbf{y}) = \frac{1}{1,000} \sum_{z=0}^{1,000} (y_k - \hat{y}_k)^2, \quad (17)$$

$$Q(\hat{\mathbf{y}}) = \frac{\max_{k \neq c}(\hat{y}_k)}{\max_c(\hat{y}_c)}, \quad (18)$$

$$\text{WD}(\hat{\mathbf{y}}, \mathbf{y}) = \inf_{\pi \in \mathcal{P}(\hat{\mathbf{y}}, \mathbf{y})} \int_{\mathbb{R} \times \mathbb{R}} |\hat{\mathbf{y}} - \mathbf{y}| d\pi(\hat{\mathbf{y}}, \mathbf{y}), \quad (19)$$

where $\mathcal{P}(u, v)$ is the set of probability distributions on $\mathbb{R} \times \mathbb{R}$ where the first factor has marginal distribution u and the second one marginal distribution v . From Table 3 to Table 9, we provide additional results regarding the transferability and required perturbation based on filtering of source images for all models considered in this study, when the adversarial examples are generated from the model that has the highest transferability to the model under inspection according to Figure 2.

F. Categorical information

In order to quantify the relation between non-targeted transferability and the categorical information, we investigate the diversity among the misclassified classes. We first group the created adversarial examples based on the category of their source images, and then find the classes into which these adversarial examples are misclassified. Following this approach, we present Figure 20, showing the percentage of the top-5 misclassified classes for each category, which are, in conjunction with the rest of the misclassified classes, adding up to 100%. We observe that, overall, 46.2% and 58.9% of the adversarial examples are incorrectly classified as one of the top-3 or top-5 misclassified classes, respectively, depending on their category of origin. Specifically, we find that, more-often-than-not, these top-5 misclassified classes are the categories semantically close to the category of the source images used, which means their prediction likelihood is close to the likelihood of the classified category itself. As such, the observations we make solidify the concerns explained in [18].

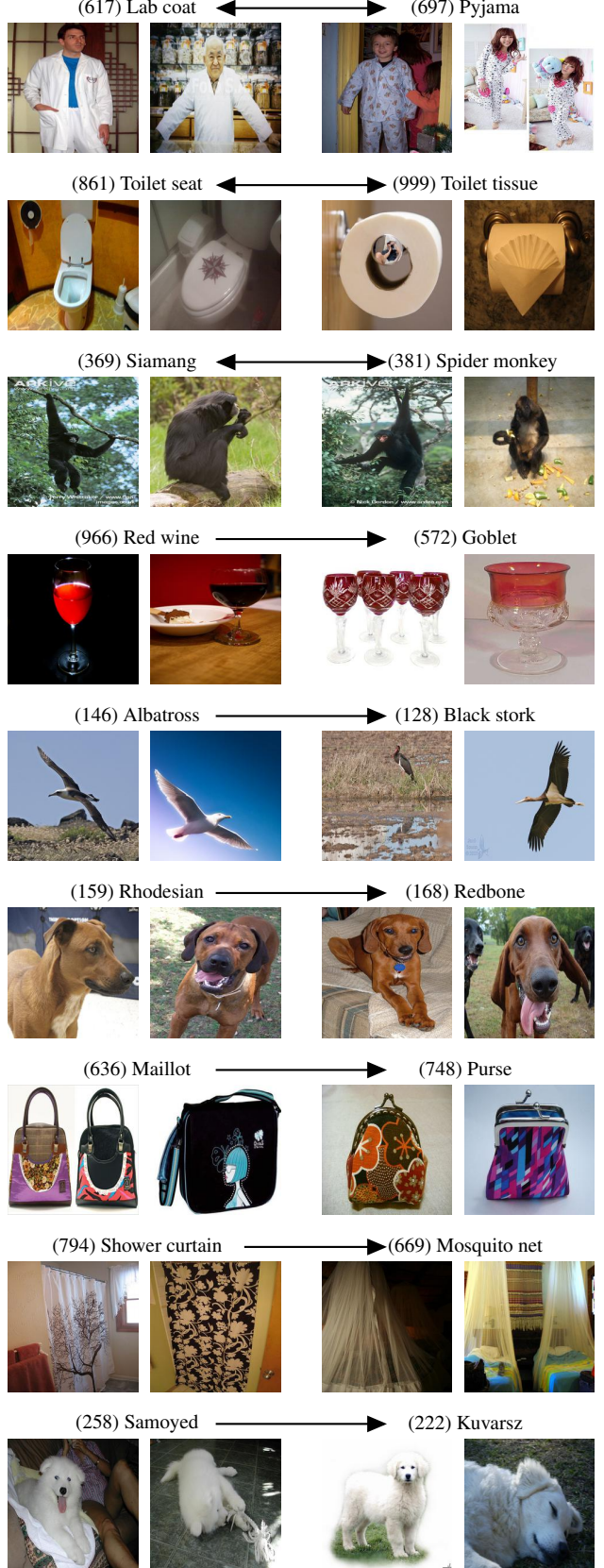


Figure 19: Adversarial examples on the left are misclassified as similar categories on the right by multiple models used in this study.

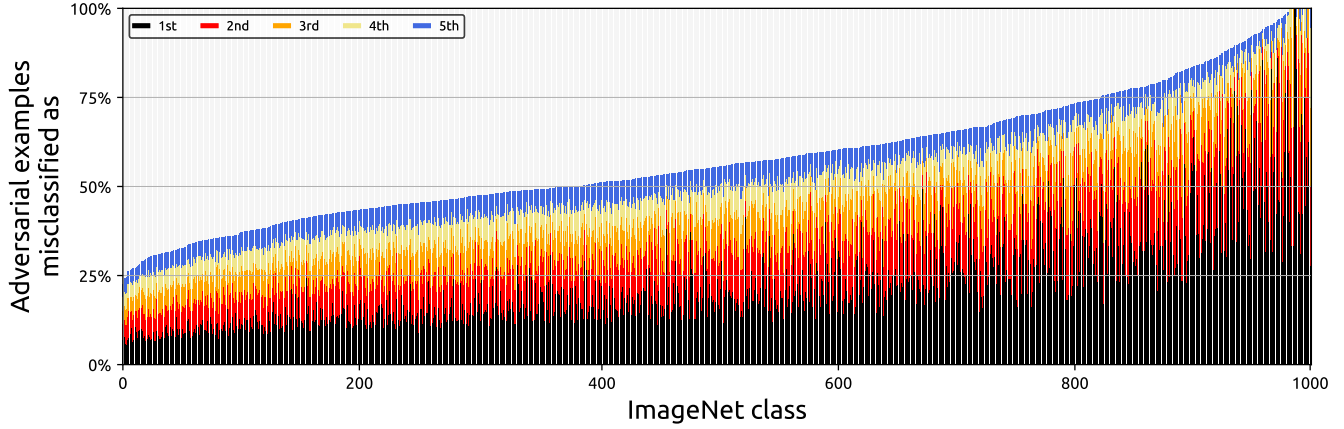


Figure 20: Percentage of the top-5 misclassified categories for adversarial examples originating from source images with classes presented on x -axis.

F.1. Semantically similar ImageNet classes

In the main text we provided a number of examples for semantically similar classes in the ImageNet dataset. In Figure 19 we expand the list of examples where the adversarial examples on the left side are classified as the classes on the right. Images in this figure as well as the ones given in the main text are taken from the ImageNet validation set.

Table 3: The lowest, the highest, and the average transferability, as well as the $L_{\{2,\infty\}}$ perturbations are provided for adversarial examples created from randomly sampled 1,000 source images 10,000 times from the datasets provided in the second row. Statistics are provided based on adversarial examples that are created from ViT-L and tested on **AlexNet**.

			All images	Hard images		Easy (fragile) images		Filtered images	
			\mathbb{S}	$\mathbb{S}_{Q<10}$	$\mathbb{S}_{Q<25}$	$\mathbb{S}_{Q>90}$	$\mathbb{S}_{Q>75}$	$\mathbb{S} \setminus (\mathbb{S}_{Q<10} \cup \mathbb{S}_{Q>90})$	$\mathbb{S} \setminus (\mathbb{S}_{Q<25} \cup \mathbb{S}_{Q>75})$
Source images in set:			19,025	1,904	4,758	1,904	4,758	15,219	9,511
Transferability	PGD	Low	28.1%	0.4%	2.2%	85.4%	71.0%	26.7%	25.8%
		Avg	34.2%	1.7%	4.7%	88.2%	75.1%	31.5%	30.1%
		High	40.4%	1.9%	6.2%	90.9%	79.4%	36.1%	33.4%
	CW	Low	6.1%	0.0%	0.0%	58.7%	36.3%	9.1%	2.3%
		Avg	12.5%	0.0%	0.2%	62.4%	41.5%	10.1%	4.0%
		High	18.2%	0.0%	0.6%	66.2%	48.0%	12.3%	5.1%
Perturbation (L_2 / L_∞)	PGD	Low	7.15 / 0.07	7.81 / 0.09	9.08 / 0.10	5.43 / 0.04	6.40 / 0.06	8.04 / 0.09	8.71 / 0.10
		Avg	7.52 / 0.08	9.76 / 0.12	9.58 / 0.12	5.70 / 0.05	6.73 / 0.06	8.59 / 0.09	9.01 / 0.10
		High	8.50 / 0.09	11.3 / 0.14	10.75 / 0.13	5.95 / 0.05	7.01 / 0.07	9.07 / 0.10	9.52 / 0.11
	CW	Low	2.35 / 0.07	— / —	2.58 / 2.58	2.12 / 0.06	2.31 / 0.07	2.78 / 0.08	2.93 / 0.09
		Avg	2.69 / 0.08	— / —	2.95 / 0.13	2.23 / 0.07	2.54 / 0.07	3.15 / 0.08	3.41 / 0.09
		High	3.11 / 0.09	— / —	4.11 / 0.14	2.37 / 0.07	2.75 / 0.08	3.41 / 0.09	3.78 / 0.10

Table 4: The lowest, the highest, and the average transferability, as well as the $L_{\{2,\infty\}}$ perturbations are provided for adversarial examples created from randomly sampled 1,000 source images 10,000 times from the datasets provided in the second row. Statistics are provided based on adversarial examples that are created from AlexNet and tested on **SqueezeNet**.

			All images	Hard images		Easy (fragile) images		Filtered images	
			\mathbb{S}	$\mathbb{S}_{Q<10}$	$\mathbb{S}_{Q<25}$	$\mathbb{S}_{Q>90}$	$\mathbb{S}_{Q>75}$	$\mathbb{S} \setminus (\mathbb{S}_{Q<10} \cup \mathbb{S}_{Q>90})$	$\mathbb{S} \setminus (\mathbb{S}_{Q<25} \cup \mathbb{S}_{Q>75})$
Source images in set:			19,025	1,904	4,758	1,904	4,758	15,219	9,511
Transferability	PGD	Low	41.2%	3.9%	9.1%	92.5%	82.8%	41.9%	39.6%
		Avg	47.8%	5.6%	13.0%	94.0%	86.6%	47.3%	45.8%
		High	54.8%	7.2%	16.9%	96.4%	90.2%	51.2%	50.4%
	CW	Low	61.3%	22.4%	34.3%	95.3%	90.8%	63.5%	65.5%
		Avg	68.4%	26.3%	38.7%	97.0%	93.2%	70.0%	69.0%
		High	74.2%	30.7%	44.4%	98.2%	96.0%	73.5%	73.1%
Perturbation (L_2 / L_∞)	PGD	Low	6.72 / 0.05	8.97 / 0.09	8.73 / 0.09	4.48 / 0.03	5.63 / 0.04	7.55 / 0.07	8.03 / 0.07
		Avg	7.34 / 0.06	9.61 / 0.10	9.28 / 0.10	4.73 / 0.03	5.95 / 0.04	7.93 / 0.07	8.38 / 0.07
		High	7.91 / 0.07	10.2 / 0.11	9.84 / 0.11	4.98 / 0.03	6.29 / 0.05	8.30 / 0.08	8.60 / 0.08
	CW	Low	7.61 / 0.11	10.4 / 0.14	10.26 / 0.14	4.35 / 0.09	5.99 / 0.11	8.34 / 0.12	8.97 / 0.12
		Avg	8.37 / 0.13	11.3 / 0.14	10.82 / 0.14	4.65 / 0.09	6.04 / 0.11	8.86 / 0.13	9.23 / 0.13
		High	9.05 / 0.13	11.8 / 0.14	11.35 / 0.14	4.94 / 0.10	6.48 / 0.12	9.35 / 0.13	9.61 / 0.13

Table 5: The lowest, the highest, and the average transferability, as well as the $L_{\{2,\infty\}}$ perturbations are provided for adversarial examples created from randomly sampled 1,000 source images 10,000 times from the datasets provided in the second row. Statistics are provided based on adversarial examples that are created from DenseNet-121 and tested on **VGG-16**.

			All images	Hard images		Easy (fragile) images		Filtered images	
			\mathbb{S}	$\mathbb{S}_{Q<10}$	$\mathbb{S}_{Q<25}$	$\mathbb{S}_{Q>90}$	$\mathbb{S}_{Q>75}$	$\mathbb{S} \setminus (\mathbb{S}_{Q<10} \cup \mathbb{S}_{Q>90})$	$\mathbb{S} \setminus (\mathbb{S}_{Q<25} \cup \mathbb{S}_{Q>75})$
Source images in set:			19,025	1,904	4,758	1,904	4,758	15,219	9,511
Transferability	PGD	Low	27.2%	3.2%	7.3%	72.0%	56.4%	27.4%	28.5%
		Avg	33.6%	5.4%	10.2%	75.4%	61.4%	31.9%	31.4%
		High	39.8%	7.5%	14.4%	78.9%	66.3%	36.1%	36.0%
	CW	Low	12.2%	0.1%	1.4%	51.5%	33.5%	9.4%	9.6%
		Avg	16.7%	0.8%	2.8%	55.8%	38.6%	13.8%	12.7%
		High	21.6%	1.5%	4.7%	60.1%	43.8%	18.3%	16.5%
Perturbation (L_2 / L_∞)	PGD	Low	6.33 / 0.05	7.95 / 0.09	7.87 / 0.08	4.80 / 0.04	5.61 / 0.05	7.06 / 0.06	7.23 / 0.06
		Avg	6.93 / 0.06	8.56 / 0.09	8.53 / 0.09	5.06 / 0.04	5.98 / 0.05	7.44 / 0.07	7.62 / 0.07
		High	7.41 / 0.08	9.16 / 0.10	8.86 / 0.10	5.30 / 0.04	6.32 / 0.06	7.84 / 0.08	7.98 / 0.07
	CW	Low	2.66 / 0.07	3.93 / 0.08	3.06 / 0.08	2.96 / 0.06	2.55 / 0.07	3.08 / 0.08	3.22 / 0.08
		Avg	3.10 / 0.08	4.75 / 0.10	3.74 / 0.10	2.46 / 0.07	2.77 / 0.07	3.41 / 0.08	3.52 / 0.08
		High	3.50 / 0.09	5.31 / 0.14	4.35 / 0.11	2.61 / 0.08	3.00 / 0.08	3.74 / 0.09	3.82 / 0.09

Table 6: The lowest, the highest, and the average transferability, as well as the $L_{\{2,\infty\}}$ perturbations are provided for adversarial examples created from randomly sampled 1,000 source images 10,000 times from the datasets provided in the second row. Statistics are provided based on adversarial examples that are created from DenseNet-121 and tested on **ResNet-50**.

			All images	Hard images		Easy (fragile) images		Filtered images	
			\mathbb{S}	$\mathbb{S}_{Q<10}$	$\mathbb{S}_{Q<25}$	$\mathbb{S}_{Q>90}$	$\mathbb{S}_{Q>75}$	$\mathbb{S} \setminus (\mathbb{S}_{Q<10} \cup \mathbb{S}_{Q>90})$	$\mathbb{S} \setminus (\mathbb{S}_{Q<25} \cup \mathbb{S}_{Q>75})$
Source images in set:			19,025	1,904	4,758	1,904	4,758	15,219	9,511
Transferability	PGD	Low	23.9%	5.2%	6.9%	65.8%	50.1%	22.3%	21.5%
		Avg	29.4%	7.4%	9.8%	69.2%	55.8%	27.1%	25.9%
		High	35.2%	9.8%	13.1%	72.8%	61.2%	32.6%	30.6%
	CW	Low	10.3%	0.8%	1.6%	43.8%	29.0%	8.7%	8.4%
		Avg	15.0%	1.7%	3.2%	48.6%	33.7%	12.4%	11.5%
		High	19.8%	2.8%	5.2%	52.5%	39.2%	16.1%	15.2%
Perturbation (L_2 / L_∞)	PGD	Low	6.41 / 0.06	7.50 / 0.08	7.47 / 0.08	5.28 / 0.04	5.86 / 0.05	6.97 / 0.07	7.09 / 0.07
		Avg	6.97 / 0.07	8.01 / 0.09	8.10 / 0.09	5.54 / 0.05	6.25 / 0.06	7.39 / 0.08	7.52 / 0.08
		High	7.50 / 0.08	8.53 / 0.10	8.65 / 0.10	5.78 / 0.06	6.49 / 0.06	7.09 / 0.08	7.93 / 0.08
	CW	Low	2.77 / 0.07	2.95 / 0.08	2.97 / 0.8	2.42 / 0.05	2.68 / 0.07	3.15 / 0.09	3.22 / 0.09
		Avg	3.21 / 0.08	3.41 / 0.09	3.58 / 0.9	2.59 / 0.06	2.91 / 0.07	3.50 / 0.09	3.58 / 0.09
		High	3.66 / 0.10	3.89 / 0.10	4.36 / 0.11	2.75 / 0.07	3.18 / 0.08	3.83 / 0.10	3.90 / 0.10

Table 7: The lowest, the highest, and the average transferability, as well as the $L_{\{2,\infty\}}$ perturbations are provided for adversarial examples created from randomly sampled 1,000 source images 10,000 times from the datasets provided in the second row. Statistics are provided based on adversarial examples that are created from ResNet-50 and tested on **DenseNet-121**.

			All images	Hard images		Easy (fragile) images		Filtered images	
			\mathbb{S}	$\mathbb{S}_{Q<10}$	$\mathbb{S}_{Q<25}$	$\mathbb{S}_{Q>90}$	$\mathbb{S}_{Q>75}$	$\mathbb{S} \setminus (\mathbb{S}_{Q<10} \cup \mathbb{S}_{Q>90})$	$\mathbb{S} \setminus (\mathbb{S}_{Q<25} \cup \mathbb{S}_{Q>75})$
Source images in set:			19,025	1,904	4,758	1,904	4,758	15,219	9,511
Transferability	PGD	Low	21.3%	3.2%	4.7%	69.7%	50.8%	19.9%	18.3%
		Avg	27.7%	5.4%	7.8%	73.2%	57.4%	24.8%	22.9%
		High	34.0%	7.5%	10.7%	77.7%	63.0%	29.7%	27.0%
	CW	Low	9.1%	0.3%	0.7%	47.9%	47.9%	7.2%	6.7%
		Avg	13.6%	1.2%	1.9%	52.7%	52.7%	10.5%	8.7%
		High	19.1%	2.3%	3.4%	56.6%	56.6%	14.0%	12.0%
Perturbation (L_2 / L_∞)	PGD	Low	6.09 / 0.06	7.08 / 0.07	7.15 / 0.07	4.83 / 0.04	5.60 / 0.05	6.86 / 0.07	7.10 / 0.07
		Avg	6.74 / 0.07	7.88 / 0.08	7.91 / 0.08	5.11 / 0.04	5.96 / 0.05	7.31 / 0.07	7.51 / 0.07
		High	7.35 / 0.08	8.62 / 0.09	8.58 / 0.09	5.37 / 0.05	6.30 / 0.06	7.75 / 0.08	7.93 / 0.08
	CW	Low	2.44 / 0.07	2.02 / 0.06	2.66 / 0.07	2.18 / 0.06	2.18 / 0.06	2.83 / 0.08	2.88 / 0.08
		Avg	2.85 / 0.08	3.03 / 0.08	3.39 / 0.09	2.32 / 0.06	2.32 / 0.06	3.18 / 0.09	3.21 / 0.09
		High	3.27 / 0.09	4.11 / 0.10	3.99 / 0.11	2.46 / 0.07	2.46 / 0.07	3.53 / 0.09	3.58 / 0.09

Table 8: The lowest, the highest, and the average transferability, as well as the $L_{\{2,\infty\}}$ perturbations are provided for adversarial examples created from randomly sampled 1,000 source images 10,000 times from the datasets provided in the second row. Statistics are provided based on adversarial examples that are created from ViT-L and tested on **ViT-B**.

			All images	Hard images		Easy (fragile) images		Filtered images	
			\mathbb{S}	$\mathbb{S}_{Q<10}$	$\mathbb{S}_{Q<25}$	$\mathbb{S}_{Q>90}$	$\mathbb{S}_{Q>75}$	$\mathbb{S} \setminus (\mathbb{S}_{Q<10} \cup \mathbb{S}_{Q>90})$	$\mathbb{S} \setminus (\mathbb{S}_{Q<25} \cup \mathbb{S}_{Q>75})$
Source images in set:			19,025	1,904	4,758	1,904	4,758	15,219	9,511
Transferability	PGD	Low	61.7%	48.1%	49.9%	83.2%	76.5%	60.7%	61.0%
		Avg	67.2%	52.6%	54.4%	86.0%	80.8%	66.6%	66.5%
		High	74.0%	57.1%	60.3%	89.0%	84.7%	71.4%	71.1%
	CW	Low	20.6%	9.5%	9.4%	52.8%	40.3%	19.9%	19.5%
		Avg	26.7%	12.3%	13.4%	56.9%	45.5%	24.7%	23.9%
		High	33.4%	15.2%	17.5%	61.4%	50.4%	29.5%	28.3%
Perturbation (L_2 / L_∞)	PGD	Low	6.49 / 0.06	7.40 / 0.07	7.38 / 0.07	4.94 / 0.04	5.57 / 0.05	6.81 / 0.06	6.87 / 0.06
		Avg	6.93 / 0.07	7.71 / 0.07	7.70 / 0.08	5.21 / 0.04	5.98 / 0.05	7.14 / 0.07	7.20 / 0.07
		High	7.35 / 0.07	8.03 / 0.08	8.04 / 0.08	5.54 / 0.05	6.34 / 0.06	7.47 / 0.07	7.54 / 0.07
	CW	Low	2.39 / 0.07	2.64 / 0.08	2.58 / 0.07	1.98 / 0.06	2.20 / 0.06	2.54 / 0.08	2.63 / 0.08
		Avg	2.64 / 0.08	2.87 / 0.08	2.88 / 0.08	2.11 / 0.06	2.37 / 0.07	2.77 / 0.09	2.82 / 0.08
		High	2.91 / 0.09	3.12 / 0.09	3.15 / 0.09	2.31 / 0.07	2.55 / 0.08	2.99 / 0.09	3.05 / 0.09

Table 9: The lowest, the highest, and the average transferability, as well as the $L_{\{2,\infty\}}$ perturbations are provided for adversarial examples created from randomly sampled 1,000 source images 10,000 times from the datasets provided in the second row. Statistics are provided based on adversarial examples that are created from ViT-B and tested on **ViT-L**.

			All images	Hard images		Easy (fragile) images		Filtered images	
			\mathbb{S}	$\mathbb{S}_{Q<10}$	$\mathbb{S}_{Q<25}$	$\mathbb{S}_{Q>90}$	$\mathbb{S}_{Q>75}$	$\mathbb{S} \setminus (\mathbb{S}_{Q<10} \cup \mathbb{S}_{Q>90})$	$\mathbb{S} \setminus (\mathbb{S}_{Q<25} \cup \mathbb{S}_{Q>75})$
Source images in set:			19,025	1,904	4,758	1,904	4,758	15,219	9,511
Transferability	PGD	Low	38.7%	23.2%	27.7%	69.2%	57.9%	38.8%	37.8%
		Avg	44.7%	27.5%	32.2%	72.8%	63.0%	43.5%	42.0%
		High	51.2%	30.8%	37.2%	77.4%	69.7%	47.3%	45.4%
	CW	Low	9.4%	2.0%	2.9%	40.1%	25.8%	10.1%	8.7%
		Avg	14.6%	3.8%	5.3%	44.2%	30.8%	13.5%	11.0%
		High	19.2%	5.4%	8.0%	49.7%	35.7%	17.7%	14.2%
Perturbation (L_2 / L_∞)	PGD	Low	6.00 / 0.05	6.79 / 0.07	6.67 / 0.06	4.68 / 0.03	5.31 / 0.04	6.27 / 0.06	6.41 / 0.06
		Avg	6.49 / 0.06	7.14 / 0.07	7.10 / 0.07	4.98 / 0.04	5.67 / 0.05	6.76 / 0.06	6.88 / 0.06
		High	7.01 / 0.07	7.54 / 0.08	7.49 / 0.08	5.26 / 0.04	6.01 / 0.05	6.98 / 0.07	7.14 / 0.07
	CW	Low	1.88 / 0.06	2.09 / 0.08	2.13 / 0.07	1.72 / 0.05	1.85 / 0.06	2.08 / 0.06	2.02 / 0.06
		Avg	2.25 / 0.08	2.56 / 0.09	2.53 / 0.08	1.85 / 0.05	2.05 / 0.06	2.42 / 0.07	2.40 / 0.07
		High	2.71 / 0.09	2.91 / 0.10	2.84 / 0.09	1.94 / 0.06	2.87 / 0.07	2.74 / 0.08	2.63 / 0.07